JGR Earth Surface

RESEARCH ARTICLE
10.1029/2018JF004880

Spatially Variable Increase in Rock Uplift in the Northern U.S. Cordillera Recorded in the Distribution of River Knickpoints and Incision Depths

Nate A. Mitchell[1] **and Brian J. Yanites**[1]

[1]Department of Earth and Atmospheric Sciences, Indiana University, Bloomington, IN, USA

Key Points:
- Knickpoint elevations and incision depths of individual tributaries in the Clearwater and Salmon watersheds increase from north to south
- Bedrock river morphologies indicate that a spatially variable increase in rock uplift caused the dissection of a low-relief paleolandscape
- We support our findings with numerical model simulations and a review of previous analytical work on transient bedrock river behavior

Supporting Information:
- Supporting Information S1

Correspondence to:
N. Mitchell,
natemitc@indiana.edu

Citation:
Mitchell, N. A., & Yanites, B. J. (2019). Spatially variable increase in rock uplift in the northern U.S. Cordillera recorded in the distribution of river knickpoints and incision depths. *Journal of Geophysical Research: Earth Surface*, *124*, 1238–1260. https://doi.org/10.1029/2018JF004880

Received 14 SEP 2018
Accepted 26 MAR 2019
Accepted article online 29 MAR 2019
Published online 23 MAY 2019
Corrected 25 JUN 2019

This article was corrected on 25 JUN 2019. See the end of the full text for details.

Abstract Landscape evolution is driven by factors like tectonics and climate, and unraveling such factors can reveal the history recorded in landscape morphology. The northern U.S. Cordillera features many potential drivers, such as the Yellowstone plume, the extrusion of a large igneous province, and the drainage of large lakes. Among this complex geologic history, the drivers of transient incision in the Clearwater and Salmon watersheds of central Idaho are not well understood. To constrain the pattern of regional incision, we analyze the morphologies of 80 individual tributaries underlain by single lithologies. From north to south across our study area, knickpoint elevations increase from about 800 to 2,200 m, and incision depths increase from about 300 to 1,200 m. We use both numerical and analytical models to demonstrate that such a gradient could represent spatial variations in rock uplift. These findings suggest that transience is driven by a spatially variable increase in rock uplift that has disrupted a low-relief paleolandscape, and the high steepness values of main drainages suggest that high rock-uplift rates are still maintained to the present. Changes in rock uplift may be related to interactions between the Yellowstone plume and the lithosphere, although base level fall from the drainage of the Lake Idaho down the proto-Snake River may be superimposed over these patterns in rock uplift. We show that careful, quantitative analyses of river profiles in geologically complex regions can differentiate between the influences of rock uplift and far-field base level changes.

1. Introduction

Landscapes form due to the uplift, erosion, and transport of rocks, and these processes bridge an array of fields including tectonics, geodynamics, climate science, and hydrology (Bishop, 2007; Whipple, 2004; Willett, 1999). Because landscapes represent the interactions of these disparate phenomena, they record changes over time through both depositional (Olsen, 1997) and erosional (Whittaker, 2012) systems. Our ability to extract information from erosional systems like bedrock rivers has improved markedly in recent decades (Bishop, 2007; Whipple, 2004; Whipple et al., 2013). Indeed, bedrock rivers have become an active area of research because they are amenable to simple theory (Whipple & Tucker, 1999) and sensitive to tectonics (Wobus et al., 2006), climate (Murphy et al., 2016), and rock properties (Bursztyn et al., 2015; Duvall et al., 2004; Gallen, 2018). Because of this sensitivity to rock properties, understanding the drivers of landscape transience in settings with variable lithology can be difficult. We explore how the distribution of river knickpoints can distinguish between underlying causes of landscape transience in central Idaho (Figure 1), a region with a wide range of lithologies (Figure 2).

Knickpoints are discontinuities in river profiles that can represent either (1) spatial changes in conditions like rock uplift or substrate properties or (2) temporal changes in factors like rock uplift or base level fall (Wobus et al., 2006). Following such temporal changes, knickpoints can migrate upstream, transmitting information about base level throughout a catchment (Niemann et al., 2001). A growing body of literature has shown that knickpoint distributions contain information regarding landscape character and history (Berlin & Anderson, 2007; Bishop et al., 2005; Crosby & Whipple, 2006; Harkins et al., 2007; Miller et al., 2013; Niemann et al., 2001; Wobus et al., 2006). For example, Whittaker and Boulton (2012) studied knickpoints upstream of normal faults in both Turkey and Italy. These authors found that knickpoint migration rates and the resulting spatial distributions are strongly dependent on fault throw rates, indicating that the magnitudes of tectonic perturbations control the timescales of transient responses. In another example, Carretier et al. (2006) studied the drivers of knickpoints along rivers in the southern Upper Rhine Graben.

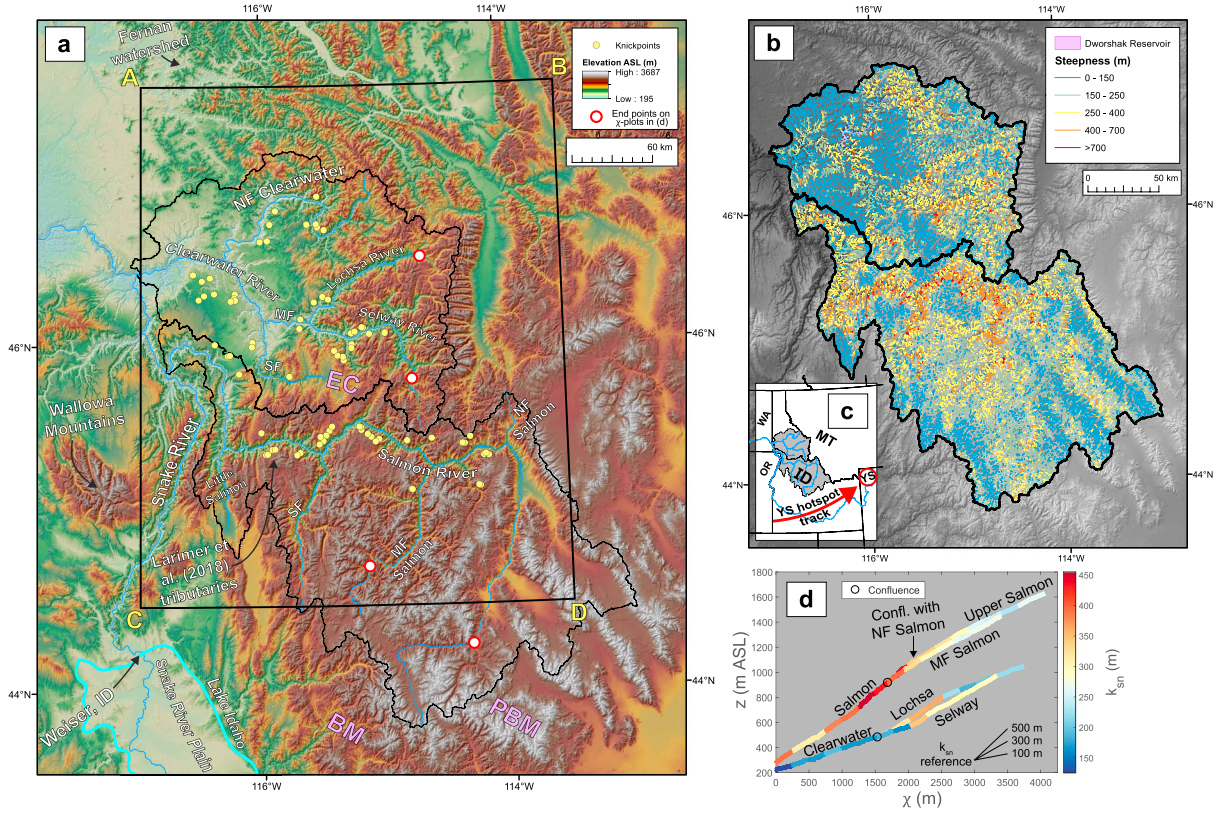

Figure 1. (a) Topography of the study area shown with the 80 identified knickpoints. Major rivers are indicated, with NF, MF, and SF representing north, middle, and south forks. Reference frame A-B-C-D is used in Figures 7–10. The locations of the Pioneer-Boulder Mountains, Boise Mountains, and Elk City are shown with PBM, BM, and EC, respectively. (b) Normalized steepness (k_{sn}) values across the Clearwater and Salmon watersheds extending down to threshold areas of 1 km^2. Note the high k_{sn} for deeply incised valleys and low for high elevation, relict surfaces. The Dworshak Reservoir is highlighted in purple because it would otherwise show deceptively low k_{sn} values. (c) Inset showing the watersheds (gray), state boundaries (ID, MT, WA, and OR for Idaho, Montana, Washington, and Oregon), and the general path of the Yellowstone (YS) hotspot track (red). (d) χ-plots for main drainages including the Salmon, MF Salmon, Clearwater, Lochsa, and Selway Rivers. End points along each river are shown in (a) as red circles.

By modeling the rivers' evolution, these authors found that these knickpoints were likely driven by rock uplift variations associated with anticline growth. Miller et al. (2013) found that knickpoints within the Susquehanna watershed in the central North American Appalachians may have been generated by base level changes around 3.5 Ma. These authors suggested that these changes could be related to mantle dynamics driving epeirogenic uplift. Similarly, Gallen et al. (2013) used knickpoints in the Southern Appalachians to demonstrate that transience lasting since the Miocene may be related to epeirogenic uplift driven by mantle forcing. Knickpoints have also been used to highlight the importance of rock properties during transient adjustment (Bishop & Goldrick, 2010; Gallen, 2018). Such applications of bedrock river theory to real landscapes have shown that knickpoints can be used to understand the various factors driving landscape evolution. We extend these approaches to central Idaho, a region where transient incision is clearly ongoing (Larimer et al., 2018; Meyer & Leidecker, 1999; Morriss & Wegmann, 2017) but the drivers of this incision are not well constrained.

In this study, we investigate the spatial distribution of (1) knickpoint elevations and (2) incision depths within the Clearwater and Salmon watersheds (Figure 1). Our goal here is to find if these morphological metrics can reveal the drivers of landscape transience in central Idaho. Is incision caused by far-field base level fall (e.g., gradual decay of long-lived high topography), drainage reorganization, or recent changes in rock uplift? Based on previous work (Larimer et al., 2018; Vogl et al., 2014), we anticipate that both spatial patterns in rock uplift and variations in rock properties have the potential to influence knickpoint migration in this region. To help distinguish between these differing effects, we (1) present example numerical models demonstrating how knickpoint elevations depend on both rock properties influencing stream power model

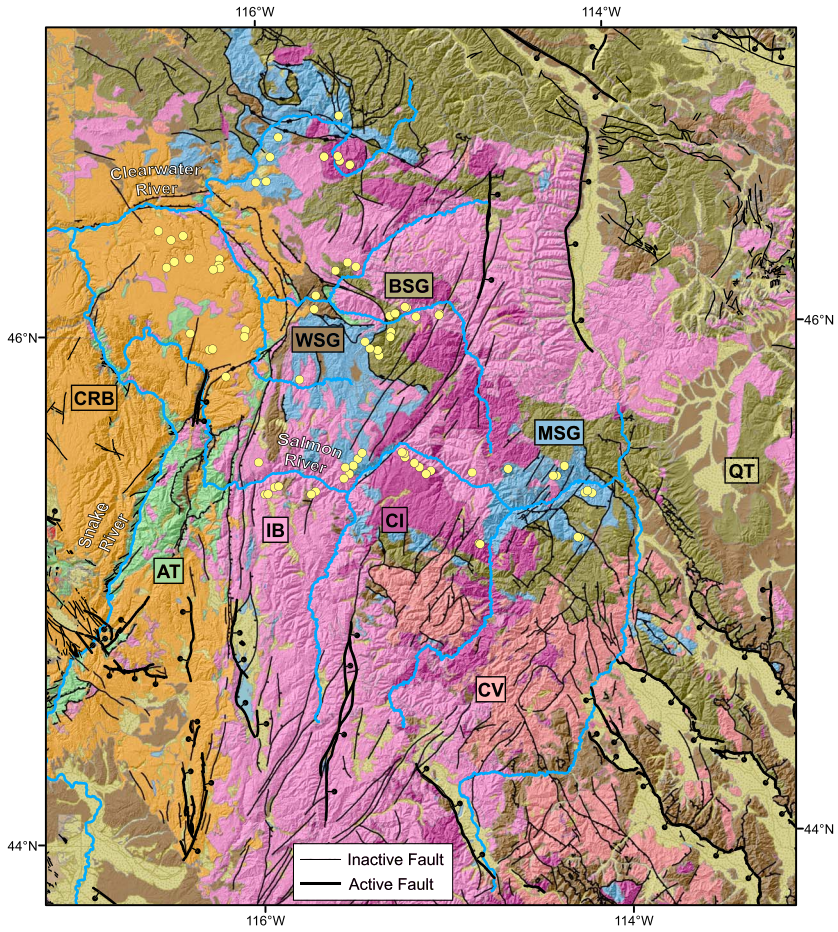

Figure 2. Lithologies within the study area (Lewis et al., 2012). Faults are shown in black. Major units include the following: (1) quartzites and siltites of the Belt Supergroup (BSG); (2) Mesoproterozoic schist and gneiss (MSG); (3) quartzites of the Windmere Supergroup (WSG); (4) accreted terranes (AT); (5) granitoids of the Idaho Batholith (IB) and Challis Magmatic Complex (CI); (6) felsic to intermediate volcanics of the Challis Magmatic Complex (CV); and (7) Columbia River Basalts (CRB). Alluvium is shown in dotted yellow (QT). Active faults are shown in bold and defined by the United States Geological Survey's Quaternary Fold and Fault Database (2018).

parameters (Whipple & Tucker, 1999) and spatiotemporal patterns in either rock uplift or base level fall and (2) highlight previous analytical work by Royden and Perron (2013) as a framework for understanding transient bedrock river behavior. Our results show that landscape transience in central Idaho is inconsistent with a far-field base level fall and more consistent with a spatially variable increase in rock uplift, although a combination of drivers is possible.

2. Background

2.1. Bedrock River Morphology

Bedrock river profiles are often described by the stream power model (Howard, 1994; Howard & Kerby, 1983; Whipple & Tucker, 1999):

$$\frac{\delta z}{\delta t} = U(x,t) - K(x,t)A(x,t)^m \left|\frac{\delta z}{\delta x}\right|^n \quad (1)$$

where z is elevation $[L]$, t is time $[T]$, x is distance upstream $[L]$, U is rock-uplift rate $[L/T]$, K is bedrock erodibility $[L^{1-2m}/T]$, A is drainage area $[L^2]$, $|\delta z/\delta x|$ is channel slope, and m and n are exponents that depend on erosion physics and the scaling of both channel width and discharge with drainage area (Whipple & Tucker, 1999). As a 1-D approximation, this relationship implicitly assumes power law dependences of both

discharge and channel width on drainage area (Whipple & Tucker, 1999); these dependences are widely observed (Montgomery & Gran, 2001; Wohl & David, 2008), although the dynamic adjustment of channel width remains an outstanding issue (Finnegan et al., 2005; Lague, 2014; Turowski et al., 2009; Whittaker et al., 2007; Whittaker & Boulton, 2012; Yanites, 2018; Yanites et al., 2010).

From equation (1), the morphology of a steady-state channel $\left(\frac{dz}{dt} = 0\right)$ with uniform conditions is as follows:

$$\frac{dz}{dx} = \left(\frac{U}{K}\right)^{1/n} A(x)^{-m/n} = k_s A(x)^{-\theta} \tag{2}$$

where k_s is channel steepness $[L^{2m/n}]$ and θ is channel concavity. This relationship of decreasing channel slope with increasing drainage area is widely observed (Flint, 1974; Hack, 1973; Howard & Kerby, 1983; Wobus et al., 2006) and serves as the basis for slope-area analysis. Based on stream power analysis, the ratio of m/n is thought to vary from ~0.35 to 0.6 and influence equilibrium channel concavity, θ (Whipple & Tucker, 1999). Concavity values measured in slope-area analysis can vary outside the expected range for m/n, however, due to disequilibrium conditions, spatially variable U or K, or a departure from detachment-limited behavior due to the inclusion of alluvial reaches (Whipple & Tucker, 1999).

Channel steepness k_s (Figure 3) is a measure of channel slope normalized by the contributing drainage area (Duvall et al., 2004; Wobus et al., 2006). This normalization removes the tendency for channel slopes to decrease downstream and allows erosive potential to be compared between rivers of different sizes. Steepness can vary due to (1) spatial changes in rock properties, climate, or rock-uplift rates or (2) transient incision following changes in climate, base level, or rock uplift (Duvall et al., 2004; Harkins et al., 2007; Perron & Royden, 2013; Wobus et al., 2006). Such changes in climate or rock uplift would be manifested as changes in K or U in equation (1), respectively.

The integral method (Perron & Royden, 2013) minimizes the influence of noise inherent in topographic data. Separating variables in equation (2) and integrating from position upstream of base level x_b ($x = 0$ m) to x yields (Mudd et al., 2014; Perron & Royden, 2013):

$$z(x) = z(x_b) + \left(\frac{U}{K{A_0}^m}\right)^{1/n} \chi = z(x_b) + k_s {A_0}^{-m/n} \chi \tag{3}$$

$$\chi = \int_{x_b}^{x} \left(\frac{A_0}{A(x)}\right)^{m/n} dx \tag{4}$$

A_0 is a reference drainage area (here set to 10^6 m^2) and χ is transformed distance upstream [L]. A graph of z versus χ is called a "χ-plot." Steady-state reaches with uniform conditions tend to have linear χ-plots, where the slope of the relationship is ${k_s A_0}^{-m/n}$. When channels are transient or have nonuniform conditions, however, equation (3) only applies within specific reaches (Figure 3). The ratio m/n can be found either (1) as the value that maximizes the R^2 of a linear regression between z and χ (Perron & Royden, 2013) or (2) through analyzing the collinearity of tributaries and trunk channels in χ-plots (Hergarten et al., 2015; Mudd et al., 2018). Steepness can be derived using either slope-area methods or χ-plots (Duvall et al., 2004; Perron & Royden, 2013; Wobus et al., 2006), and each method has certain advantages (Wang et al., 2017).

Evaluating channel morphology with equations (2)–(4) is only possible after delineating the transition from hillslope to channel processes. This transition is thought to occur where slope begins to decrease with increasing drainage area (Montgomery & Foufoula-Georgiou, 1993). The drainage area at this location is called the critical drainage area (A_{cr}) and represents a threshold between either (1) divergent and convergent topography or (2) debris-flow and fluvial processes, with higher drainage areas dominated by fluvial processes (Montgomery & Foufoula-Georgiou,1993; Tarboton et al., 1991; Whipple & Tucker, 1999; Wobus et al., 2006). A_{cr} values generally range from 10^5 to 10^6 m^2 (Montgomery & Foufoula-Georgiou,1993; Tarboton et al., 1991).

The exponent for channel slope in equation (1) (n) strongly influences the transient behavior of bedrock rivers (Royden & Perron, 2013; Tucker & Whipple, 2002). The value of n is postulated to reflect dominant incision processes, with erosion by plucking consistent with n values of ~2/3 to 1 and erosion by abrasion

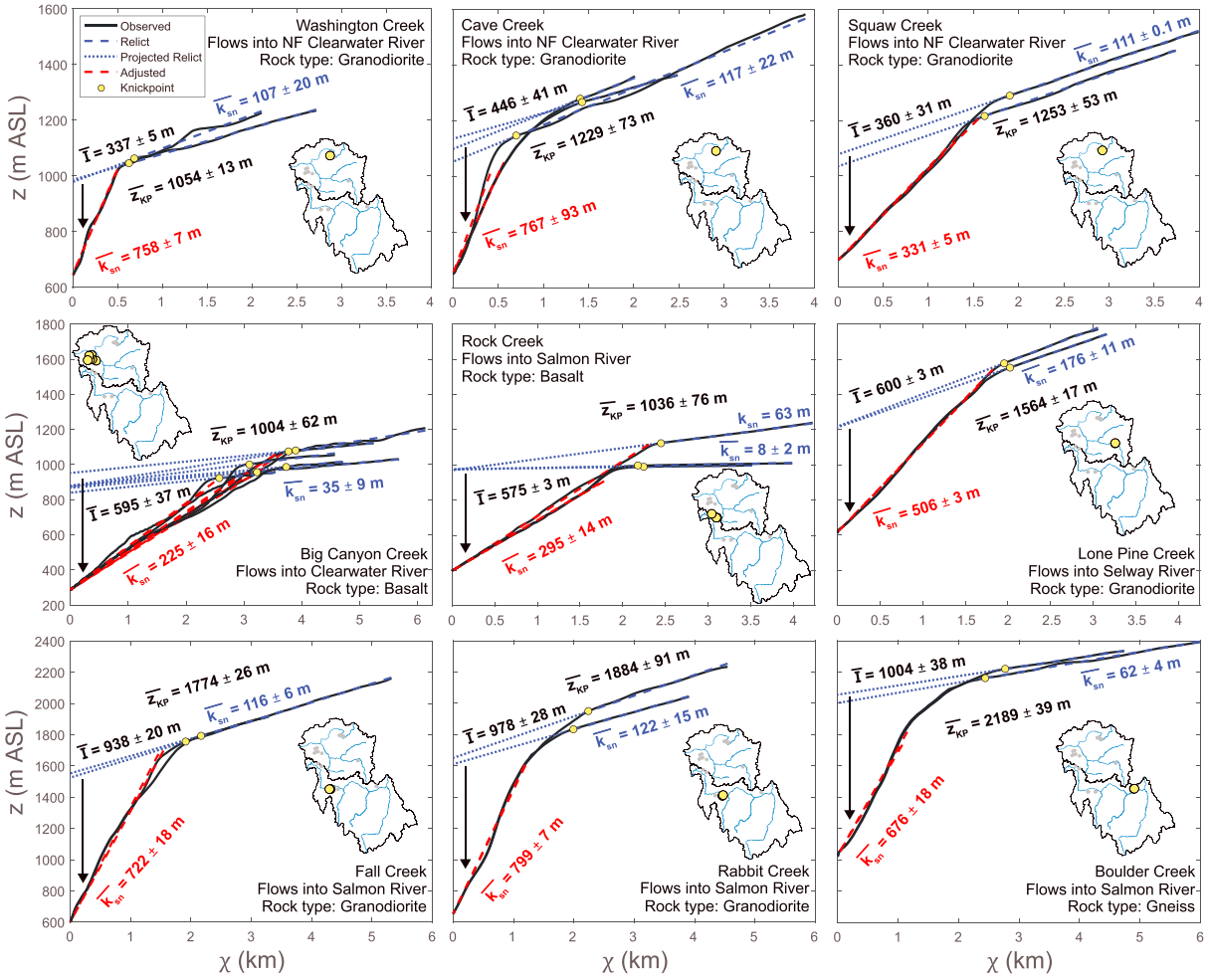

Figure 3. χ-plots demonstrating the morphological metrics assessed here: knickpoint elevations (z_{KP}), steepness values (k_{sn}) of relict and adjusted reaches, and incision depths (I). Average values of these metrics are shown with standard deviations for each group of tributaries. The location of each stream is shown in an inset map.

consistent with n values of ~5/3 (Whipple et al., 2000). Because incision processes are controlled by bedrock properties like jointing (Hancock et al., 1998) and tensile strength (Sklar & Dietrich, 2001), recognizing potential variations in the exponent n is important in our lithologically diverse study area. The exponent n may also be influenced by discharge variability (Lague, 2014), which likely varies across our study area. To illustrate how such variations in n can influence knickpoint distributions, we utilize a previous work (Royden & Perron, 2013) that reduces the complications of knickpoint migration arising from equation (1) to simpler relationships.

2.2. Analytical Models of Transient Behavior and Knickpoint Celerity

The analytical version of the stream power model provided by Royden and Perron (2013) provides a useful framework for understanding transient behavior and knickpoint celerity in response to rock uplift and lithology. This analytical model utilizes the migration of slope patches (i.e., base level signals) to solve for bedrock river elevations over time. Because (1) the model framework may be conceptually unfamiliar for many readers and (2) the following section relies on this model, we present a review of the model in section S1 of the supporting information.

For the solutions presented below, we assume spatially uniform conditions (K, m, and n). Following a sustained, spatially uniform increase in rock-uplift rates from U_1 to U_2, the χ-space distances (χ_{KP}) of these

knickpoints upstream of base level are as follows (Royden & Perron, 2013):

$$\chi_{KP}(t) = \begin{cases} \dfrac{nU_1 t}{\left(\frac{U_1}{K}\right)^{1/n} A_0^{-m/n}} & for\ n < 1 \quad (5a) \\ KtA_0^{m/n} & for\ n = 1 \quad (5b) \\ \dfrac{t(U_2 - U_1)}{\left(\left(\frac{U_2}{K}\right)^{1/n} - \left(\frac{U_1}{K}\right)^{1/n}\right) A_0^{-m/n}} & for\ n > 1 \quad (5c) \end{cases}$$

From equations (5a)–(5c), knickpoints' horizontal celerities are shown to be constant in χ-space, making them a power law function of drainage area and variable in real space. Note that a knickpoint's horizontal celerity is dependent on U_2 only when $n > 1$ (equation (5c)).

Using the framework of Royden and Perron (2013), we have derived relationships for knickpoint elevations (z_{KP}) assuming uniform conditions for a step increase in rock-uplift rate:

$$z_{KP}(t) = \begin{cases} z(\chi_b) + t(U_2 + (n-1)U_1) & for\ n < 1 \quad (6a) \\ z(\chi_b) + U_2 t & for\ n = 1 \quad (6b) \\ z(\chi_b) + t(U_2 - U_1)\left(\dfrac{\left(\frac{U_2}{K}\right)^{1/n}}{\left(\frac{U_2}{K}\right)^{1/n} - \left(\frac{U_1}{K}\right)^{1/n}}\right) & for\ n > 1 \quad (6c) \end{cases}$$

Unlike horizontal knickpoint celerities, vertical celerity is constant in both χ-space and real space (Niemann et al., 2001). Note that for a sustained increase in rock uplift and uniform conditions, knickpoint vertical celerity depends on erodibility, K, only when $n > 1$ (equation (6c)) while knickpoint horizontal celerity always depends on K (equations (5a)–(5c)). Vertical and horizontal knickpoint migration rates have different relationships with rock-uplift rates, n, and K, and these differences can be exploited in the interpretation of real landscapes.

Transient incision depths are defined here as the difference between the initial and current elevation at a tributary's outlet, where the initial elevation is estimated using the relict k_{sn} (Figure 3). Incision depths can also be predicted from equations (5a)–(5c) and (6a)–(6c). For a sustained increase in rock-uplift rate (or base level fall) and all other conditions being steady and uniform, the elevation of the relict profile projected downstream to the outlet ($z_{\text{rel proj}}$) [L] is as follows:

$$z_{\text{rel proj}} = z_{\text{KP}} - \left(\frac{U_1}{K}\right)^{1/n} A_0^{-m/n} \chi_{\text{KP}} \quad (7)$$

Incision depth I [L] at a stream's outlet is then found as follows:

$$I(t) = z_{\text{rel proj}} - z(\chi_b) = t(U_2 - U_1) \quad (8)$$

In each n scenario, the difference between this projected relict elevation and the current elevation at the outlet, $z(\chi_b)$, simplifies to only $t(U_2 - U_1)$. This result exemplifies why, for transience caused entirely by increased rock uplift, transient incision depths should reflect a minimum surface uplift of the relict landscape (rock uplift minus relict exhumation, where rock uplift is U_2 and relict exhumation equals U_1; England & Molnar, 1990) since incision began at the stream's outlet. Surface uplift is only tracked by incision depths after incision begins at the outlet because, for example, a small tributary within the relict landscape could experience surface uplift before the knickpoint arrives at the tributary's outlet.

These solutions apply to a sustained increase in rock-uplift rates, but the Royden and Perron model can also be applied to situations where rock uplift varies over time. Because a wide range of temporal

variations are possible, we only focus on a simple scenario where conditions (K, m, and n) are spatially uniform and rock-uplift rates (or base level fall rates) increase from U_1 to U_2 for a duration of t_p before returning to U_1. Here $t = 0$ when the increase in rock uplift begins and $t = t_p$ when it ends, so these solutions only apply for $t > t_p$. When $n \leq 1$, χ_{KP} can still be solved with equations (5a) and (5b) and z_{KP} can be solved as follows:

$$z_{KP} = nU_1 t + t_p(U_2 - U_1) + z(\chi_b) \tag{9}$$

We do not focus on the solution for $n > 1$ because the location of the knickpoint is then strongly dependent on the duration and magnitude of increased rock uplift (i.e., the knickpoint is not located at a specific slope patch). As in equation (8), these z_{KP} values can again be used to calculate incision depths:

$$I = t_p(U_2 - U_1) \tag{10}$$

In this situation, incision depths are constant with time and only dependent on the duration of increased rock uplift (t_p) and the difference between U_2 and U_1. The differences between equations (6a)–(6c), (8), (9), and (10) highlight the fact that different base level histories result in different bedrock river morphologies, and a combination of steepness values, knickpoint elevations, and incision depths can be exploited to discriminate between potential drivers of incision.

Figure 4 shows examples of transience driven by a sustained increase in rock-uplift rates from 0.05 to 0.3 mm/year, while Figure 5 shows examples of transience driven by a temporary increase in rock-uplift rates from 0.05 to 0.55 mm/year. We use three different n values (0.67, 1, and 1.5), take m as $0.5 \cdot n$, and vary K to demonstrate its influence on knickpoint propagation. All examples show the initial profile (gray) and the profile after 4 Myr of adjustment, and the temporary increase in rock-uplift rates in Figure 5 lasts for the first 2 Myr of adjustment ($t_p = 2$ Myr). In each figure, (a)–(f) are analytical solutions (Royden & Perron, 2013) using fixed K values. To show how climate change might influence transient behavior, (g)–(i) of each figure are numerical solutions where K either increases or decreases gradually over the 4-Myr duration to the K value that would provide either double or half the horizontal knickpoint celerity of the constant K scenario ("Const. K"), respectively. We present our approach to scaling K values below. The constant K scenarios use the K values shown in (a)–(c) for the corresponding n scenario, and these numerical and analytical solutions agree quite well. The small differences between the numerical and analytical scenarios' knickpoint elevations are due in part to numerical diffusion and the manual selection of knickpoints in the numerical model results.

We present these examples to demonstrate the following: (1) knickpoint elevations depend on both rock-uplift rates and n values, as shown by equations (6a)–(6c) and (9); (2) different base-level histories can produce the same incision depths and knickpoint elevations (e.g., compare scenarios in Figures 4 and 5), but steepness variations along the profiles can still discriminate between these scenarios (i.e., reduction in lower reaches' steepness following the return to $U = 0.05$ mm/year at $t = 2$ Myr in Figure 5); (3) knickpoint elevations and incision depths are still equal for each n scenario when K is different but held constant (Figures 4a–4f and 5a–5f); and (4) temporal variations in K can cause differences in knickpoint elevations and estimated incision depths (Figures 4g–4i and 5g–5i). Note that this last point is due to the balance between rock uplift and erosion during temporal changes in K. The variations in knickpoint elevations and incision depths following temporal changes in K in Figures 4g–4i and 5g–5i are still rather small when $n \leq 1$, however. We further address the role of temporal changes in K in section 5. When K values are different but held temporally constant (Figures 4a–4f and 5a–5f), knickpoint elevations do not change because an increase in horizontal celerity is offset by a corresponding reduction in steepness.

Here we review our approach to scaling K values with the Royden and Perron (2013) analytical model. Using a known K value for a given n value (K_A and n_A) and equations (5a)–(5c), one can solve for the K values that would produce comparable horizontal knickpoint migration rates for a different parameter set (K_B and n_B) and given rock-uplift rates (U_1 and U_2). If C_A and C_B are the parameter sets' horizontal knickpoint celerities in χ-space (equations (5a)–(5c)) such that $\frac{C_B}{C_A}$ represents the horizontal knickpoint celerity of set B relative to

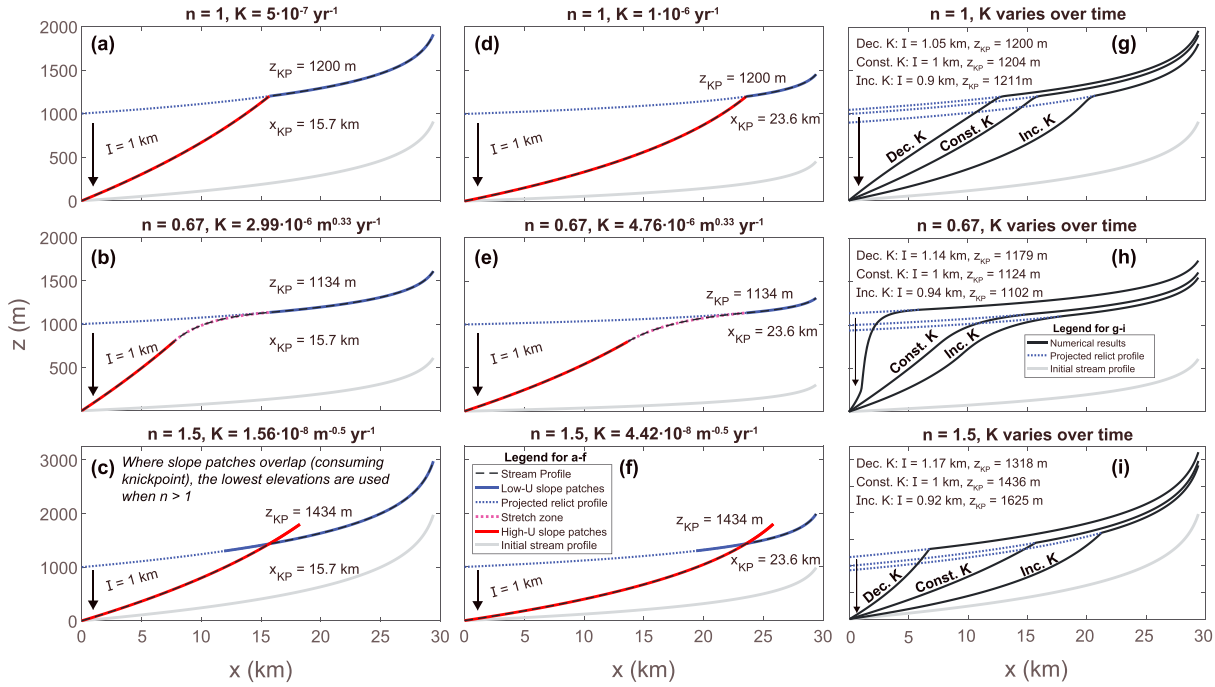

Figure 4. Analytical (a–f) and numerical (g–i) solutions to transient adjustment for 4 Myr following a sustained increase in rock-uplift rates from 0.05 to 0.3 mm/year. In (g–i), K is either held constant or linearly decreases or increases over time to a final value. The default, final lower, and final higher K values are as follows: (g) 5×10^{-7} year^{-1}, 2.5×10^{-7} year^{-1}, and 1×10^{-6} year^{-1}; (h) 2.99×10^{-6} m$^{0.33}$·year^{-1}, 1.88×10^{-6} m$^{0.33}$·year^{-1}, and 4.76×10^{-6} m$^{0.33}$·year^{-1}; and (i) 1.56×10^{-8} m$^{-0.5}$·year^{-1}, 5.53×10^{-9} m$^{-0.5}$·year^{-1}, and 4.43×10^{-8} m$^{-0.5}$·year^{-1}.

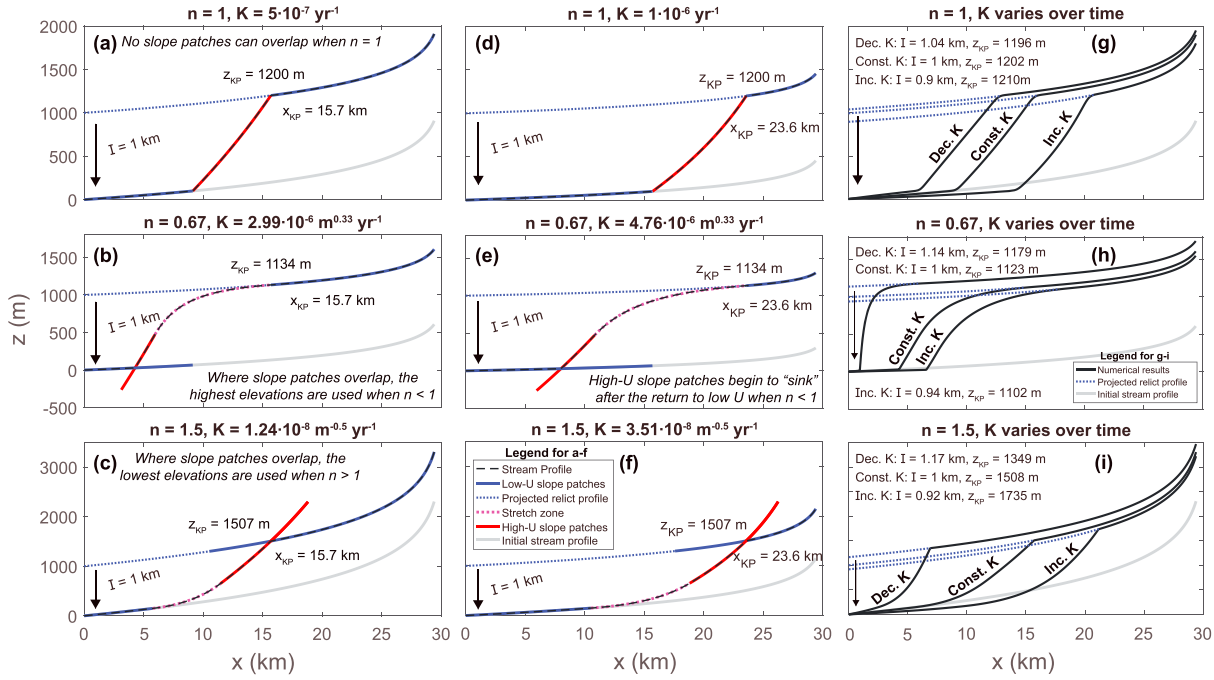

Figure 5. Analytical (a–f) and numerical (g–i) solutions to transient adjustment for 4 Myr following a temporary, 2-Myr increase in rock-uplift rates from 0.05 to 0.55 mm/year. In (g–i), K is either held constant or linearly decreases or increases over time to a final value. The K values for (g–h) are the same as in Figure 4, but here the default, final lower, and final higher K values for (i) are as follows: 1.24×10^{-8} m$^{-0.5}$·year^{-1}, 4.39×10^{-9} m$^{-0.5}$·year^{-1}, and 3.51×10^{-8} m$^{-0.5}$·year^{-1}.

that of set A, then

$$K_B = \begin{cases} \left(\frac{C_B}{C_A}\left(\frac{n_A}{n_B}\right)\left(\frac{K_A}{U_1}\right)^{1/n_A} {U_1}^{1/n_B}\right)^{n_B} & for\ n_A\ and\ n_B \le 1 \quad (11a) \\ \left(\frac{C_B}{C_A}\left(\frac{U_1}{U_2-U_1}\right)\frac{n_A}{\left(\frac{U_1}{K_A}\right)^{1/n_A}}\left({U_2}^{1/n_B}-{U_1}^{1/n_B}\right)\right)^{n_B} & for\ n_A \le 1\ and\ n_B > 1 \quad (11b) \\ \left(\frac{C_B}{C_A}\frac{{U_2}^{1/n_B}-{U_1}^{1/n_B}}{\left(\frac{U_2}{K_A}\right)^{1/n_A}-\left(\frac{U_1}{K_A}\right)^{1/n_A}}\right)^{n_B} & for\ n_A\ and\ n_B > 1 \quad (11c) \end{cases}$$

Note that these equations still assume steady and uniform characteristics (K, m, and n) and a step increase in rock-uplift rates from U_1 to U_2. Also note that these relationships may not be appropriate for a temporary pulse of incision if $n_A$and/or$n_B > 1$ due to knickpoints' sensitivity to the duration and magnitude of increased rock uplift when $n > 1$. Recall that vertical celerities (equation (6a)–(6c)) are unaffected by K when $n \le 1$, so these relationships (equations (11a)–(11c)) only change vertical knickpoint migration rates when $n > 1$ (equation (6c)). The K values in Figures 4a–4f and 5a–5f are scaled so that the lower K scenarios (a–c) have knickpoints at $\chi = 2$ km while the higher K scenarios (d–f) have twice the horizontal knickpoint celerity in χ-space and knickpoints at $\chi = 4$ km.

2.3. Background on Central Idaho

We use these mathematical descriptions of bedrock river profile evolution to explore what drives landscape evolution in central Idaho. The ongoing transient adjustment here is clear; rivers steepen dramatically as they flow from low-relief surfaces at high elevations to steep gorges along main drainages like the Salmon and Clearwater Rivers (Figure 1b).

Here we briefly review the geologic history of central Idaho to demonstrate how this history has created an excellent natural experiment in landscape evolution. The creation of the North American Cordillera during the Mesozoic and early Cenozoic (Dickinson, 2004; Saleeby, 1983) caused the granitic Idaho Batholith (IB in Figure 2) to be emplaced among Mesoproterozoic metasedimentary and meta-igneous rocks (BSG and MSG in Figure 2), Neoproterozoic and Cambrian quartzites (WSG in Figure 2), and Permian and Triassic accreted terrains (AT in Figure 2) formed of metasedimentary and volcanic island arcs (Lewis et al., 2012). During the Eocene, granitoids and felsic to intermediate volcanics of the Challis Magmatic Complex were also emplaced (CI and CV in Figure 2; Lewis et al., 2012).

The Columbia River Basalts (CRB in Figure 2) comprise a large igneous province (Coffin & Eldholm, 1994) and were extruded from about 17 to 6 Ma (V. E. Camp & Hooper, 1981) over Oregon, Idaho, and Washington. Peak extrusion rates occurred from 16.7 to 15.9 Ma, generating 95% of the total CRB volume (Kasbohm & Schoene, 2018), and were followed by declining rates and sporadic, increasingly infrequent eruptions thereafter (Camp et al., 1982). Indeed, the flows occurring from 15 to 6 Ma (Saddle Mountains Basalts) had decreasing frequencies beginning around 12 Ma (Barry et al., 2013) and constitute only 1.2% of the total CRB volume (Kasbohm & Schoene, 2018).

While this region has experienced Basin and Range extension (Sonder & Jones, 1999), the tributaries we study here are generally situated far from recent faulting (Figure 2). Basin and Range extension has been active in the southeastern regions of the Salmon watershed from as early as 17 Ma to the present, accomplishing extension in a NE-SW direction (Janecke, 1992; Janecke et al., 1991). This extension has a similar orientation as earlier Eocene extension in the same area lasting from about 48 to 20 Ma (Janecke & Blankenau, 2003). We do not study any tributaries in the vicinity of these grabens, however. After the extrusion of the CRBs, Basin and Range extension also reactivated faults along the Salmon River suture zone (Tikoff et al., 2001), the Precambrian margin of North America along which the accreted terrains were stitched to North America (Snee et al., 1984). This faulting did not extend eastward into the Idaho Batholith, however (Hamilton, 1963; Tikoff et al., 2001). Furthermore, the Quaternary fault database from the U.S. Geological Survey and Idaho Geological Survey (2018) shows no recent fault activity for most of the Clearwater and Salmon watersheds (Figure 2).

The drainage of Lake Idaho (Figure 1a) down the proto-Snake River has traditionally been considered the driver of incision in central Idaho (Meyer & Leidecker, 1999). Lake Idaho occupied a Basin and Range structure in the western Snake River Plain from about 9.5 to 1.7 Ma but spilled into the ancestral Hell's Canyon near Weiser, ID (Figure 1a) sometime between 6.4 to 1.7 Ma (Wood, 1994; Wood & Clemens, 2002). This drainage capture increased the discharges of the lower Snake River (Link et al., 2014), and the Snake River's drainage area continued to grow as the North American plate moved W-SW over the Yellowstone plume (Pierce & Morgan, 1992). A recent study by Larimer et al. (2018), however, found the erosion rates and morphologies of certain Salmon River tributaries to be inconsistent with this driver. These authors used in situ ^{10}Be concentrations of fluvial sediment to show that the erosion rates of adjusted and relict tributaries of the Salmon River near Burgdorf, ID (Figure 1a) differ by a factor of about 2.4. By calibrating best-fit incision models, these authors found that increased incision began around 9.5 ± 2 Ma and persists to the present. These findings also coincide with the threefold increase in exhumation rates around 11–8 Ma found through fission-track data in the Boise Mountains (BM in Figure 1a; Sweetkind & Blackwell, 1989) and (U-Th)/He dating in Pioneer-Boulder Mountains (PBM in Figure 1a; Vogl et al., 2014). Larimer et al. (2018) further argued that this sustained increase in erosion may be driven by density changes in the mantle-lithosphere facilitated by the Yellowstone plume. Indeed, Zhou and Liu (2019) also argued for a geodynamic source of uplift in central Idaho, with dynamic uplift around 14–11 Ma causing an ~800-m increase in elevation by the present.

Transience driven primarily by drainage capture (Yanites et al., 2013) or geodynamic phenomena (Braun, 2010) should produce distinct morphologies, and our intention is to build on the work of Larimer et al. (2018) by analyzing a larger suite of bedrock rivers distributed throughout central Idaho. By focusing on a series of individual tributaries that have incised into only one rock type, we can avoid issues from erosion across dipping contacts (Forte et al., 2016; Perne et al., 2017) and any long-wavelength patterns in rock uplift. While individual valleys in these watersheds have glacial features, their distinctive glacial morphologies (Amerson et al., 2008) allow them to be recognized and excluded from fluvial analyses. Below, we outline both (1) our approach to these fluvial analyses in central Idaho and (2) the numerical models we present to demonstrate the roles of both lithology and rock-uplift history in landscape adjustment.

3. Methods

We map the spatial distribution of knickpoints by analyzing 80 tributaries within the Clearwater and Salmon watersheds. By focusing on individual tributaries situated along much larger drainages like the Salmon River, we can isolate knickpoints within single rock types. Knickpoints are identified by discontinuities in channel profiles that manifest as breaks in either slope-area data (Wobus et al., 2006) or χ-plots (Perron & Royden, 2013). To locate knickpoints, we used Topotoolbox v2 (Schwanghart & Kuhn, 2010; Schwanghart & Scherler, 2014) to extract river profile and slope-area data from 10-m digital elevation models provided by the United States Geological Survey. Due to the noise inherent within these digital elevation models (Wobus et al., 2006), elevations along the profile were smoothed over 55 nodes. Each node is spaced either 10 or ~14.1 m apart, where the latter value corresponds with diagonal flow across a raster cell. This smoothing interval was found to minimize scatter on slope-area plots while still preserving the shape of the profile, and smoothed elevations were used for both slope-area plots and χ-plots. Specifically, we manually selected the bounds of relict and adjusted reaches for each tributary on a χ-plot, where the knickpoint elevation is the lower boundary of the relict reach (Figure 3). This same selection was then evaluated on a slope-area plot before it was accepted. Note that before we analyzed channel morphologies, A_{cr} was manually selected for each tributary as a value over 10^5 m^2 (Whipple & Tucker, 1999) defining a “roll over” in slope-area data (Montgomery & Foufoula-Georgiou,1993) such that slope starts to decrease downstream as a power law function of drainage area (equation (2)).

Because the dimensions of k_s depend on the value of θ, we use a reference concavity $\theta_{ref} = 0.5$ for m/n, consistent with other studies (Tucker & Whipple, 2002; Whittaker, 2012; Gasparini & Whipple, 2014; Han et al., 2014; Whipple, DiBiase, et al., 2017). With this reference concavity, all profiles have a normalized steepness (k_{sn}) with units of meters (Figure 3). For both relict and adjusted river channels, we identify reaches with linear relationships between z and χ consistent with a single k_{sn} value in equation (3) (Figure 3) and

power law relationships between channel slope and drainage area (Wobus et al., 2006). Low k_{sn} reaches at high elevations are interpreted to be remnants of the relict, low erosion rate landscape, while high k_{sn} reaches at lower elevations are interpreted to be adjusted to the new rate of base level lowering (driven by increased rock-uplift rates and/or incision further downstream). The knickpoint is the lowest elevation of the relict, low k_{sn} reach (Figure 3).

We also quantify the depth of incision along main drainages to constrain the magnitude and spatial patterns in rock-uplift or base level fall. Incision depths are found by projecting the relict reach downstream of the knickpoint (e.g., Schoenbohm et al., 2004) in a χ-plot and taking the difference between this projection and the modern elevation of the tributary's outlet (Figure 3). We focus on the incision depths of tributaries situated directly on main drainages, which we take as the Salmon, Clearwater, MF Clearwater, NF Clearwater, Lochsa, and Selway, and lower SF Clearwater Rivers (Figure 1a). The main drainages therefore serve as a datum to compare the spatial patterns in incision depth. Using these main drainages as a datum (rather than each individual tributary) is advantageous because the high drainage areas of main channels allow greater confidence that these channels are adjusted to new conditions (i.e., sufficiently powerful flows to keep pace with rock uplift via erosion; high A in equation (1)). If transience is caused entirely by an increase in rock-uplift rates, then incision depths at a tributary's mouth would be equal to the cumulative surface uplift at the location since the tributary's incision began, as discussed in section 2.2. If transience is instead caused by only base level fall further downstream (e.g., from the drainage of Lake Idaho), these incision depths would represent the cumulative decrease of the mainstem river's elevation.

3.1. Knickpoint Distribution in Lithologically Variable Terrain

In central Idaho, the variable lithology has the potential to influence both the erodibility (K) and incision processes (n) in these river systems. Such differences among tributaries have the potential to influence knickpoint migration and the resulting knickpoint distribution. To guide our interpretation of the distribution of knickpoints, we present a series of numerical models of bedrock river evolution (equation (1)) demonstrating how tributary knickpoints vary with time as a function of rock-uplift history in lithologically nonuniform terrain. The model is intended to provide insight into the 2D distribution of knickpoints in central Idaho, but the results have general implications for knickpoint distributions in any landscape where lithology varies across the watershed. Specifically, we show that by considering both vertical and horizontal differences in knickpoint distributions, one can tease out rock-uplift patterns even in the face of variable lithology. This capacity is enabled by the fact that vertical and horizontal celerities (equations (5a)–(5c), (6a)–(6c), and (9)) have different relationships with rock uplift, n, and K.

We use a first-order upwind finite difference scheme and assess a series of interconnected 1-D stream models (Figure 6a). We use $dx = 10$ m and $dt = 10$ years and take m as $0.5 \cdot n$. Several rivers (river 1, north fork of river 1, and river 2) are joined by small tributaries (10 km long) and flow westward to a regional drainage (river 0), crossing three lithologic units: Units A, B, and C. The contacts separating these units are taken to be vertical, as dipping contacts introduce complicated behaviors (Perne et al., 2017) that we do not intend to address in these examples. The north fork of river 1 ("1N"), river 1, and river 2 are meant to represent the North Fork Clearwater, Clearwater, and Salmon rivers, while river 0 is meant to represent the Snake River. Similarly, Units A, B, and C could be thought of as the Columbia River Basalts, the Idaho Batholith, and the Belt Group. We are not attempting to accurately recreate our study area; our intention is to use these simple models to qualitatively demonstrate spatial trends in knickpoint elevations along small tributaries given different forcings (e.g., uniform or variable rock-uplift rates and drainage capture) exerted on rivers that have spatially variable properties (K, m, and n) and an orientation roughly similar to the rivers in our study area. Any efforts to accurately represent central Idaho will require more data than are currently available (e.g., cosmogenic nuclide concentrations and thermochronology cooling ages).

We present three different forcing scenarios: (1) a spatially uniform increase in rock-uplift rates from 0.05 to 0.15 mm/year; (2) a spatially variable increase in rock-uplift rates, with rates increasing linearly toward the south ("tilting" scenario; Figure 6b); and (3) a drainage capture scenario, where regional drainage river 0 has its minimum drainage area increased by a factor of 10^5. Each scenario begins with the rivers equilibrated to the initial rock-uplift rate of 0.05 mm/year, although the drainage capture scenarios maintain $U = 0.05$ mm/year throughout the simulation as a null hypothesis representing no change in rock uplift.

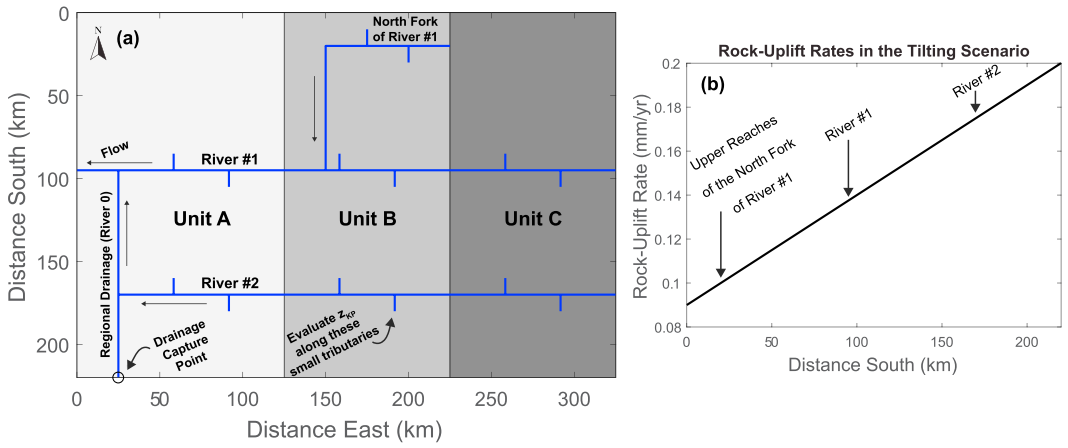

Figure 6. (a) Domain used in the numerical models. (b) Rock-uplift rates used for the tilting scenario.

The drainage capture scenario is meant to mimic the drainage of Lake Idaho down the proto-Snake River; while a step increase in drainage area is not the same as the drainage of a large lake, we use this scenario to represent a single pulse of incision rather than a sustained signal. We created drainage areas using Hack's Law (Hack, 1957):

$$A(\ell) = C\ell^h \tag{12}$$

where ℓ is distance downstream, C is a coefficient $[L^{2-h}]$, and h is an exponent. We take C and h to be 1 $m^{0.2}$ and 1.8, respectively, as these values fall within the expected ranges (Whipple & Tucker, 1999). We use critical drainage areas of 0.1 km^2 and adjust the drainage areas at the tops of river 0, river 1N, river 1, and river 2, so they are similar in magnitude to the Snake River just upstream of the Salmon River (190,000 km^2), the North Fork Clearwater River (3,500 km^2), the confluence of the Lochsa and Selway Rivers (11,000 km^2), and the confluence of the Salmon an North Fork Salmon Rivers (14,000 km^2), respectively. In the drainage capture scenario, river 0 has a drainage area of 1.9 km^2 before increasing to its default value of 190,000 km^2, and rivers 1N, 1, and 2 have lower drainage areas (3.5, 1.1, and 1.4 km^2). These changes were intended to maximize the incisional responses of rivers 1N, 1, and 2, especially as we are focusing on incision downstream of the capture point along river 0 rather than upstream of it. With their default drainage areas, rivers 1N, 1, and 2 have very low incision depths because the changes in drainage area are proportionally smaller. Furthermore, the expectations we demonstrate for drainage capture scenarios focus on generalized spatial patterns.

Although we vary the stream power model parameters used within Units A, B, and C, we do not present an exhaustive exploration of the parameter space. Instead, we focus on examples demonstrating the different roles of K, n, and rock uplift/base level fall in knickpoint migration. When K is varied, we use equations (11a)–(11c) to scale horizontal knickpoint celerities by specific proportions.

4. Results

4.1. Bedrock River Morphology

The k_{sn} values of the Salmon, Middle Fork Salmon, Clearwater, Lochsa, and Selways are shown in a χ-plot in Figure 1d (these rivers are labeled in Figure 1a). These main drainages all have relatively high k_{sn}. The lower Salmon River has an especially high k_{sn} of ~300 to 400 m, while the Clearwater River further to the north has a lower k_{sn} of ~200 m. These values are generally higher than tributaries' relict k_{sn}(e.g.,Figure 3).

We present our observations for tributaries in two formats: (1) with distance upstream of the corresponding watershed outlet (Salmon or Clearwater) and (2) with distance relative to reference frame A-B-C-D in Figure 1a. Both Figures 7 and 8 show knickpoint elevations (a and d), incision depths (b and e), and tributaries' k_{sn}values (c and f), but Figure 7 shows these metrics with distance upstream from the watershed outlet

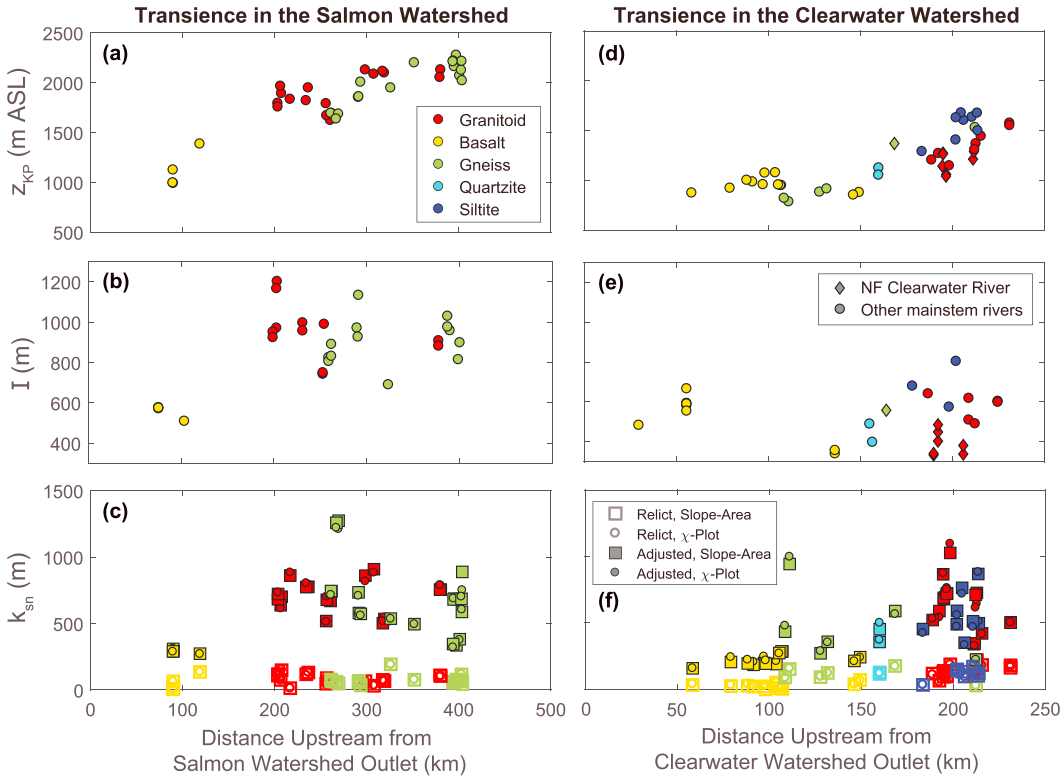

Figure 7. Knickpoint elevations (z_{KP}), incision depths (I), and steepness (k_{sn}) within the Salmon (a–c) and Clearwater (d–f) watersheds. Lithologies are labeled by color, shown in (a). z_{KP} and I values along the north fork (NF) Clearwater River (Figure 1a) are shown with diamonds.

while Figure 8 shows them relative to reference frame A-B-C-D. Figures 9 and 10 also show knickpoint elevations and incision depths, respectively, relative to the reference frame. We present tributaries' k_{sn} values, then knickpoint elevations, and finally incision depths.

Individual tributaries have a much wider range of k_{sn} values then the mainstem rivers, and differences in k_{sn} between relict and adjusted reaches of tributaries vary considerably (Figures 7 and 8). Basalt tributaries tend to have both lower k_{sn} values and lower increases in k_{sn} from relict to adjusted reaches. Otherwise, k_{sn} values for tributaries do not exhibit clear spatial relationships (Figures 7 and 8) but values from slope-area and integral methods agree extremely well here, closely following a 1:1 relationship ($k_{sn\chi} = 0.994\ k_{snSA}$, $R^2 = 0.993$; Figure S3).

Knickpoint elevations generally increase with distance upstream in both watersheds, even for tributaries underlain by the same lithology (Figure 7). The pattern of knickpoint elevations becomes clearer, however, when viewed relative to reference frame A-B-C-D (Figure 1a). Figure 8 shows knickpoint elevations to generally increase to the south/southeast across all lithologies. Figure 9 shows the elevations of both knickpoints (circles, z_{KP}) and tributaries' confluences with main drainages (triangles, z_{confl}), where the confluences are colored by the height of knickpoints above main drainages ($z_{KP} - z_{confl}$; equivalent to $z_{KP} - z(\chi_b)$ in equations (6a)–(6c) and (9)). Note that the perspective in Figures 9 and 10 is toward the southwest, such that the viewer is to the northeast of reference frame A-B-C-D (Figure 1a) and looking southwest from Montana. In these 3-D figures, each point has a shadow directly beneath it, and the positions of mainstem rivers are also shown. Figure 9 shows that both knickpoint elevations and knickpoints' heights above main drainages generally increase to the south/southeast. Note that knickpoints' heights above main drainages can be indicative of both erosion rates and the duration of transience along each tributary (similar to but not the same as incision depths), potentially indicative faster erosion and/or longer sustained adjustment to the south/southeast in Figure 9. For example, assuming uniform conditions in each individual tributary and a sustained increase in rock uplift, then $z_{KP} - z(\chi_b)$ should be linearly dependent on both t and U_2

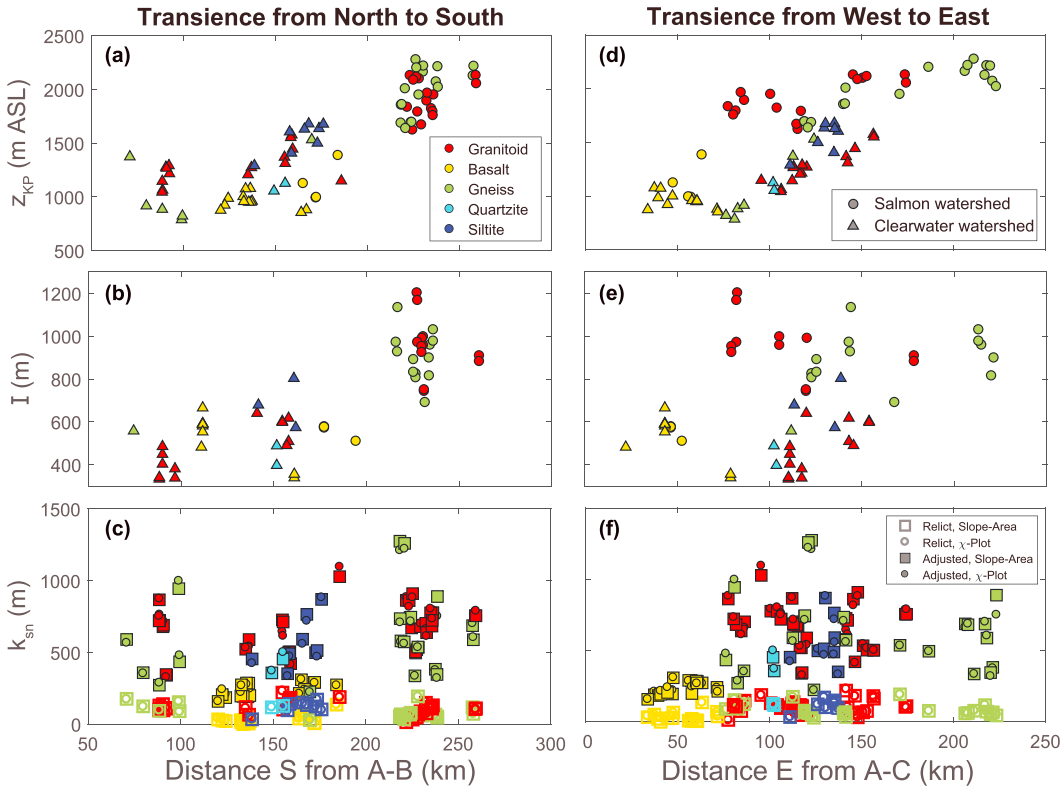

Figure 8. Knickpoint elevations (z_{KP}), incision depths (I), and steepness values (k_{sn}) with distance (a–c) south from line A-B and (d–f) distance east from line A-C. Lines A-B and A-C are shown in Figure 1a. Each tributary's lithology is shown by color. z_{KP} and I values within the Salmon and Clearwater watersheds are shown with circles and triangles, respectively. Only incision depths of tributaries situated directly on main drainages are shown (Salmon, Clearwater, MF Clearwater, NF Clearwater, Lochsa, Selway, and lower SF Clearwater Rivers).

(equations (6a)–(6c)). For a short pulse of base level fall and $n \leq 1$, then $z_{KP} - z(\chi_b)$ should increase with t_p and U_2 as well as t for $nt > t_p$ (equation (9)).

Incision depths along main drainages increase with distance upstream in the Salmon watershed (Figure 7b). Incision depths do not increase with distance upstream in the Clearwater watershed (Figure 7e) and are generally lower along the North Fork Clearwater River than at similar distances upstream along the Lochsa and Selway Rivers (around 200 km in Figure 7e). Much like the knickpoint elevations, transient incision depths also exhibit clear spatial variations when viewed relative to reference frame A-B-C-D (Figures 8 and 10). Across all lithologies and in both watersheds, incision depths generally increase to the south (Figure 8b) and exhibit no discernable pattern to the east (Figure 8e). This trend is represented by the north-dipping plane fit to the incision data in Figure 10a; for incision I (m), distance east D_E (m), and distance south D_S (m), $I = 106\ \text{m} + 3.46 \times 10^{-3} D_S - 1.14 \times 10^{-4} D_E$ ($R^2 = 0.653$). Despite the range in incision depths being 870 m in Figure 10a, most values are within 100 to 200 m of the regression (84% are in the center 4 bins in Figure 10b) and all are within 321 m of it (Figure 10c). A linear regression of incision versus distance south (not including distance east) indicates that incision along main drainages increases about 3.93 m for each kilometer southward ($R^2 = 0.70$). Note that the gray surface in Figure 10c is a plane fit to the residuals, and this plane is essentially flat. In summary, (1) knickpoint elevations generally increase with distance upstream and distance to the south/southeast while (2) incision depths increase with distance upstream along the Salmon River and distance to the south.

4.2. Numerical Models

Now, we review results from our numerical models to provide context for the transient morphologies observed in central Idaho (section 4.1). The purpose of these models is to examine the sensitivity of

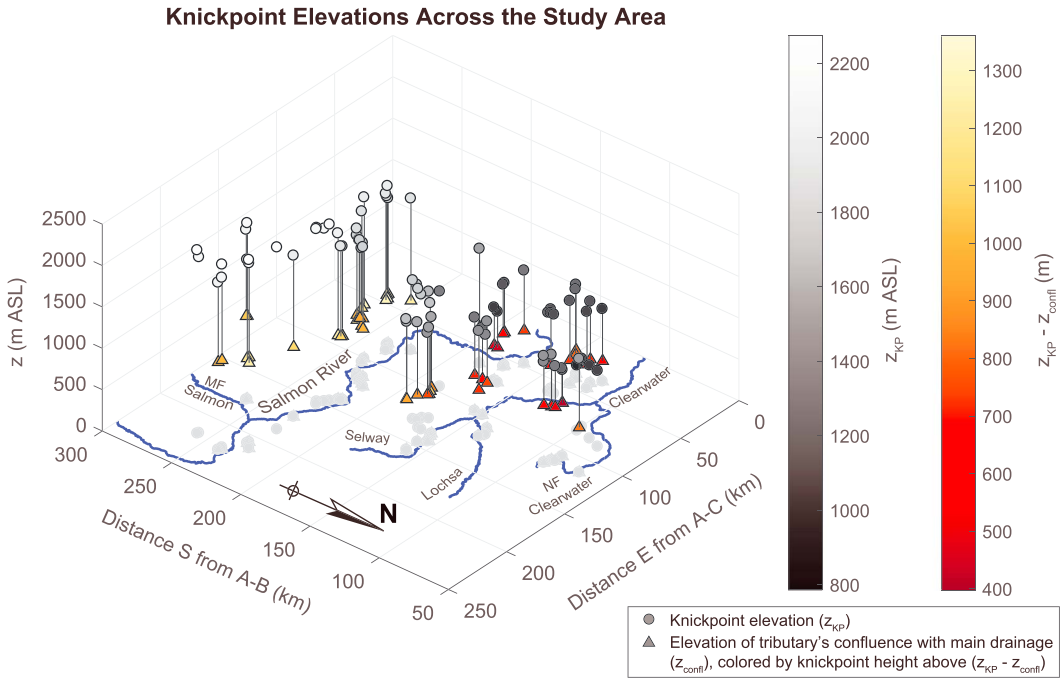

Figure 9. Elevations (z) of knickpoints (z_{KP}, circles) and tributaries' confluences with main drainages (z_{confl}, triangles) with position relative to reference frame A-B-C-D (Figure 1a). Note that z_{confl} values are positioned at modern river elevations but colored by the height of the knickpoint above them ($z_{KP} - z_{confl}$). Both knickpoint elevations and their height above main drainages generally decrease to the north. To aid in visualizing these data, each point has a shadow situated directly beneath it. Knickpoints without lines and triangles beneath them are not situated on main drainages. Note that the trend of increasing knickpoint elevations is oblique to the rivers' main orientation.

knickpoint elevations and incision depths to factors like K, n, and base level history, which are all largely unknown throughout our study area.

Figures 11 and 12a–12d show knickpoint elevations and incision depths with distance south across the model domain (Figure 6a). Symbol style denotes the unit underlaying each tributary, which we use to vary stream model parameters, while symbol size denotes time during the simulation. Four times are shown for knickpoint elevations (2.5, 5, 7.5, and 10 Myr), while only two times are shown for incision depths (5 and 10 Myr) to promote visual clarity. Results for a uniform or spatially variable ("tilting," Figure 6b) increase in rock-uplift rates are shown in Figure 11, while Figure 12 shows results from drainage capture along the regional drainage ("river 0," Figure 6a) meant to represent the Snake River.

A spatially uniform increase in rock-uplift rates (or far-field base level fall rates) creates equal knickpoint elevations over time (Figure 11), as previously shown by Niemann et al. (2001). Even if the n and K values of each unit differ, z_{KP} values are still equal for specific n values (Figure 11c). Note that the distribution of n values across the domain can be significant. For example, if n_A was 0.67 in Figure 11c, a stretch zone would develop along the mainstem rivers (Figures 4b and 4e) and influence the propagation of knickpoints into the other units upstream. Also note that knickpoint elevations for uniform uplift are consistent with equations (6a)–(6c); for example, for $n = 1$, equation (6b) predicts z_{KP} values of 375, 750, 1,125, and 1,500 m for t values of 2.5, 5, 7.5, and 10 Myr, closely matching the results in Figure 11a.

In the tilting scenario, the north-to-south increase in rock-uplift rates (Figure 6b) is mirrored in the north-to-south increase in knickpoint elevations during each time step (Figures 11e and 11g). This effect is similar to spatial variations in U_2 in equations (6a)–(6c). We use Figure 11g to demonstrate the influence of varying K values while maintaining constant n values; knickpoint elevations are the same as in Figure 11e, although knickpoints in high-K units appear and disappear earlier. This effect also applies to uniform uplift scenarios, as demonstrated in Figures 4a–4f.

In the drainage capture scenarios, knickpoint elevations are equal along river 1 and the north fork of river 1 ("1N") but higher along river 2 (Figures 12a and 12c). This north-to-south step change in knickpoint

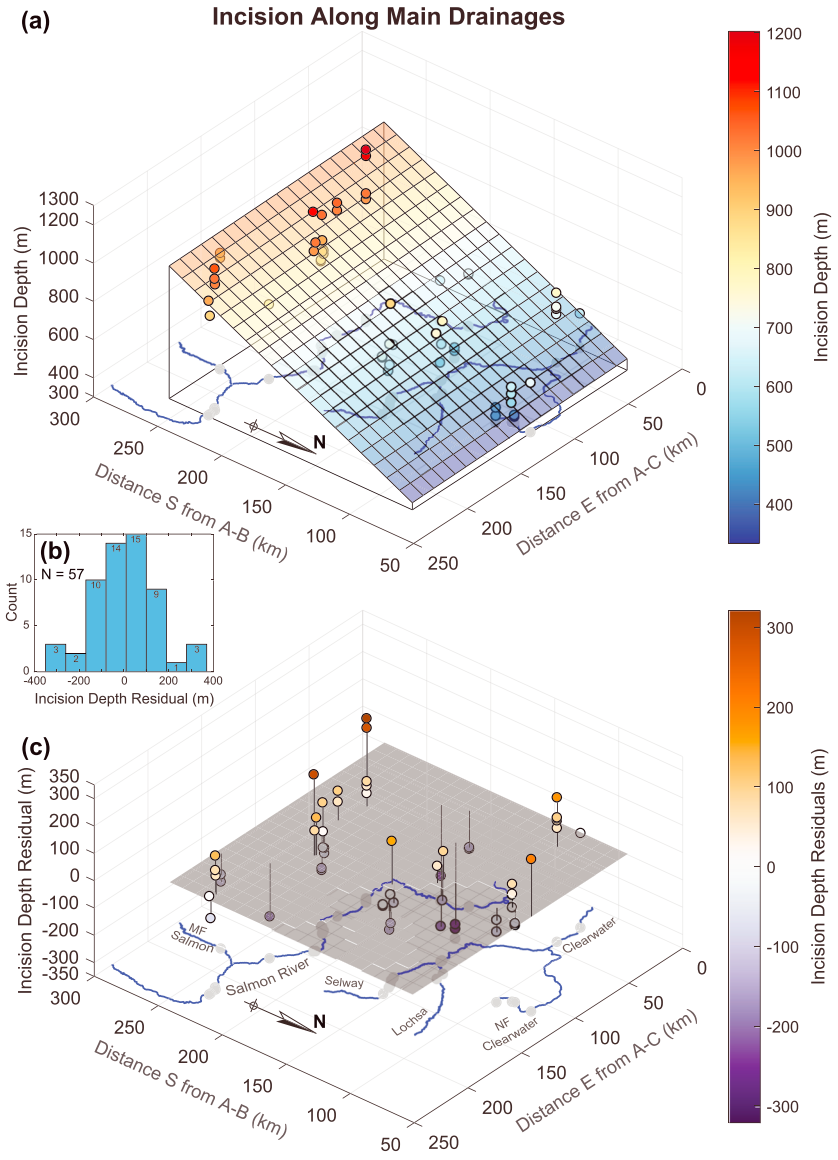

Figure 10. (a) Incision depths along mainstem rivers and with position relative to reference frame A-B-C-D (Figure 1A). Only tributaries situated directly along main drainages are shown. In both (a) and (c), gray shadows are situated directly beneath each point. A polynomial function fit to these data (dipping surface) shows that incision depths decrease to the north across these watersheds. Black lines connect each corner of the regression to better show the regression's shape. Note that the trend of increasing incision is oblique to the rivers' main orientation. (b) Histogram of the residuals from the regression shown in (a). Bins have widths of 90 m and the lower bin edges range from −350 to 280 m. (c) Spatial distribution of residuals from the regression shown in (a). The gray surface is a plane fit to the residuals, and it is essentially flat. All residuals are connected to the gray surface by black lines.

elevations is the result of both river 1 and river 1N receiving the same signal of base level fall at the confluence of river 1 and regional drainage river 0 (Figure 6a) while river 2 receives a different signal. The step change in drainage area at the top of river 0 causes diminishing incision downstream of the capture point (Figure 12e) because the increase in drainage area becomes proportionally smaller along river 0. Importantly, incision depths along river 2 are equal and constant with time as in Figure 5, even if K varies between the different units (Figure 12f).

Even during a uniform increase in rock-uplift rates, incision depths can still differ across the domain because variations in drainage area cause tributaries to have different knickpoint arrival times (t in equation (8)).

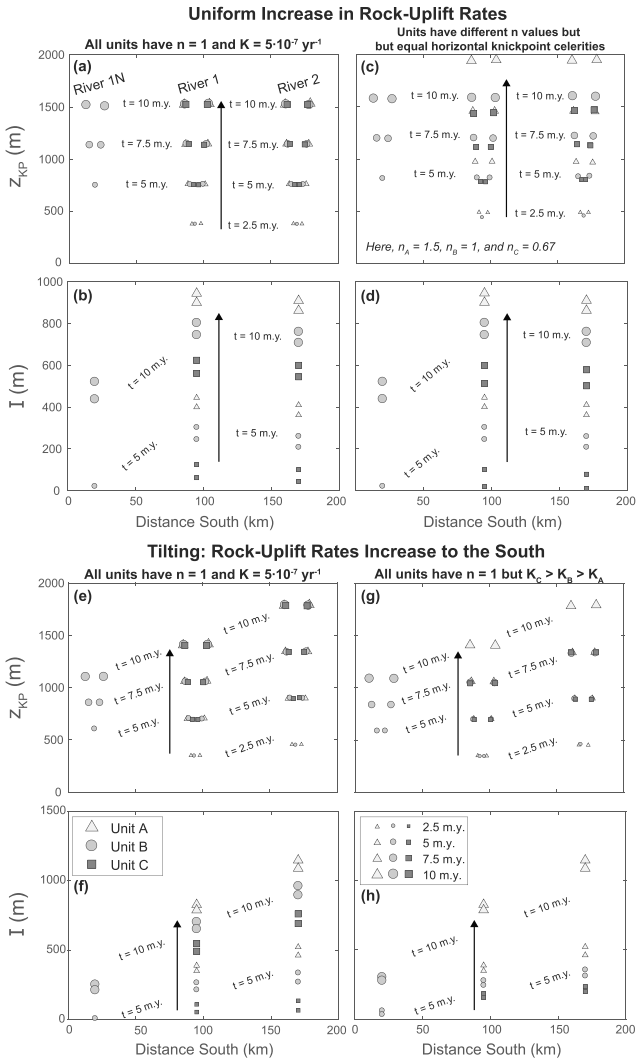

Figure 11. Knickpoint elevations (z_{KP}) and incision depths (I) from the (a–d) uniform uplift and (e-h) tilting scenarios. The values of K_A, K_B, and K_C in (c, d) are 1.98×10^{-8} $m^{-0.5}$·$year^{-1}$, 5×10^{-7} $year^{-1}$, and 2.99×10^{-6} $m^{0.33}$·$year^{-1}$, respectively, while in (g, h) they are 5×10^{-7}, 7.5×10^{-7}, and 10^{-6} $year^{-1}$.

This time delay in incision initiation causes lower incision depths along river 1N during each time step in Figures 11b and 11d. The drainage areas of rivers 1 and 2 are meant to be similar to the Clearwater and Salmon rivers, respectively, and allow for more similar incision depths over time. Although this time delay also contributes to lower incision depths along river 1N in the tilting scenarios (Figures 11f and 11h), lower incision depths are also a result of the northward decrease in rock-uplift rates. Indeed, both incision depths and knickpoint elevations in the tilting scenarios (Figures 11e–11h) exhibit north-to-south gradients reflective of the spatially variable rock-uplift rates. To summarize the results from these numerical models, knickpoint elevations and incision depths have different relationships with drivers of landscape evolution, and these differences can be exploited in the interpretation of transient landscapes. Also note that our modeling scenarios are not mutually exclusive, and a combination could be achieved (e.g., drainage capture during tilting).

5. Discussion

Landscape evolution driven by far-field base level fall, plume-lithosphere interactions, or drainage reorganization should all produce distinct morphologies, and our intention here is to evaluate if the topography of central Idaho matches the expectations for each scenario. Spatial gradients in both knickpoint elevations (Figures 7–9) and incision depths (Figures 7, 8, and 10) in central Idaho are inconsistent with an increase in far-field base level fall propagating up the Snake River, which one may expect from the gradual decay of a preexisting highland. In that scenario, knickpoint elevations would be more uniform and depend largely on the slope exponent n (Figures 11a–11d). Although incision patterns in our drainage capture scenarios (Figure 12) share some similarities with the incision pattern in central Idaho (Figures 8 and 10), incision depths along the lower reaches of the Salmon River are notably lower than the incision depths further upstream (Figure 7b). If transience throughout central Idaho is driven solely by incision along the Snake River, then one would expect incision depths to be more equal along the Salmon River (Figure 12f). This expectation would apply to incision along the Snake due to (1) the gradual or sudden drainage of Lake Idaho, the (2) gradual increase in the Snake River's drainage area as the North American plate moved W-SW over the Yellowstone plume (Pierce & Morgan, 1992), or (3) far-field base level changes. Instead, tributaries along the lower reaches of the Salmon River (Rock Creek in Figure 3) have incision depths more similar to those across the drainage divide in the Clearwater watershed (Big Canyon and Lone Pine Creek in Figure 3). This distinction may reflect a forcing that extends across watershed boundaries, like rock uplift or climate.

Before we expand on the roles of rock uplift and climate, it is important to first note in the context of drainage capture that a temporary pulse of increased base level fall should cause k_{sn} values to decrease following the signal's passage (Figure 5). Instead, the mainstem Salmon River maintains a high steepness of about 300 to 400 m from its outlet to its confluence with the North Fork Salmon River (Figure 1d), with slight variations due in part to changes in lithology. Similarly, the other main drainages shown in Figure 1d all have relatively high steepness values that generally exceed 200 m. Following either a brief pulse of increased rock uplift or incision along the Snake, these rivers would have returned to a lower steepness once either (1) the rock uplift pulse ended or (2) the wave of incision due to base level fall along the Snake had swept through these main drainages. Additionally, all of the tributaries studied here (Figures 1–3) have steep lower reaches that must be maintained through a sustained increase in base level fall. If increased rock uplift drives transience here, this interpretation does not mean that rock uplift has not varied over time; instead, it suggests that relatively

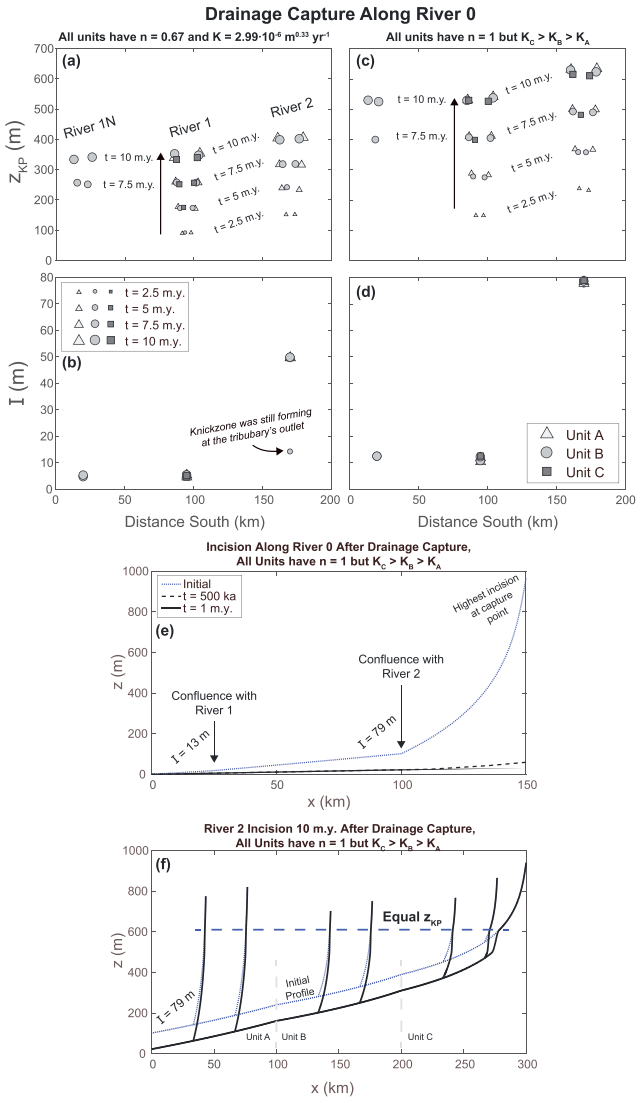

Figure 12. (a–d) Knickpoint elevations (z_{KP}) and incision depths (I) from the drainage capture scenarios. (e–f) Incision along rivers 0 (e) and 2 (f) following drainage capture along regional drainage river 0 (minimum drainage area increased by a factor of 10^5 at the capture point in Figure 6a). The values of K_A, K_B, and K_C in (c–f) are 5×10^{-7}, 7.5×10^{-7}, and 10^{-6} year^{-1}, respectively.

high rock uplift is likely maintained to the present. A real-world example of the relationship between k_{sn} and local rock uplift has been documented along Dragon's Back pressure ridge in California (Hilley & Arrowsmith, 2008). Situated along the San Andreas Fault, a pressure ridge created by right-lateral transpression causes rock uplift to increase and decrease as drainage basins are carried to the NW across the feature. This setting allows for excellent space-for-time substitution, and Hilley and Arrowsmith (2008) showed that channel steepness accurately tracks rock-uplift rates with rapid response times (~6.6 kyr in their study area). While the exact response times of the large mainstem rivers in central Idaho to changes in local rock uplift are unknown, the mainstem rivers have large drainage areas (A in equation (1)) that aid in providing short response times. The relatively rapid response of river steepness to the initiation and cessation of increased rock uplift (or base level fall) allows us to infer that, due to the high k_{sn} values of main drainages (Figures 1b and 1d), the region continues to experience either high rock uplift or high base level fall from further downstream.

Now, we return to the ever-present issue in tectonic geomorphology: the role of climate in landscape evolution. With the highlands of the Salmon watershed featuring more valleys with glacial features, it may be possible for climate variations to influence incision and knickpoint propagation here (Figures 4g–4i and 5g–5i). Goren (2016) developed an analytical model demonstrating the potential for climate fluctuations to influence river profiles but also emphasized that high-frequency,low-amplitude climate oscillations like Milankovitch cycles are unlikely to have a lasting influence on detachment-limited bedrock rivers. Furthermore, relating specific factors like mean runoff or discharge variability (DiBiase & Whipple, 2011) directly to erodibility amid other factors like rock properties remains a challenge. In addition to understanding the roles of pertinent climatic factors, reliable records of these factors over geologic time and at sufficient temporal resolutions may remain elusive. Perhaps climate fluctuations have had a larger impact on horizontal knickpoint migration than knickpoint elevations and incision depths, as shown for $n \leq 1$ in Figures 4g–4h and 5g–5h. If climate fluctuations are significant enough to cause the observed gradients in knickpoint elevations and incision depths through, for example, isostatic uplift (Molnar & England, 1990), then central Idaho may be among the most significant examples of such a feedback mechanism.

Conversely, an increase in rock uplift would satisfy many observations in central Idaho. High modern U would sustain the high k_{sn} observed along main drainages and tributaries, and either higher $U$and/or a longer sustained increase in U to the south (t in equations (6a)–(6c) and (8)) would cause the higher knickpoint elevations and incision depths. In such a scenario, differential uplift could have disrupted and caused incision into a formerly continuous paleolandscape (Whipple, Forte, et al., 2017). The cosmogenic ^{10}Be relict erosion rates (~0.05 mm/year) obtained by Larimer et al. (2018) closely match both (1) cosmogenic ^{10}Be erosion rates further north in the Fernan watershed (~0.03 to 0.07 mm/year; Parker, 2016; Figure 1a) and (2) the long-term exhumation rates of 0.05 to 0.06 mm/year since 78 Ma estimated from ^{40}Ar/^{39}Ar cooling ages near Elk City, ID (EC in Figure 1a; Lund et al., 1986). This similarity could suggest that remnant relict surfaces were previously continuous with the lower relief landscape to the north. In that case, the plane shown in Figure 10a may provide insight into the resulting surface uplift, with deviations due in part to knickpoint arrival times; if all the transience is driven by enhanced rock uplift, incision equals the difference between rock uplift and relict exhumation rate (equation (8)). If U or t are even higher in the southern Salmon watershed, perhaps the area's relict landscape has already been obliterated. Nevertheless, changes in the Snake River's incision due to drainage capture

(Wood & Clemens, 2002) could still be an important consideration. Indeed, a combination of drivers could be at work, with increased base level fall along the Snake superimposed over spatial variations in rock uplift.

Spatial contrasts in erosion rate following an increase in U could also promote divide migration, and such a capture event was proposed within the Salmon watershed by Beranek et al. (2006). Distinctive chert and quartzite clasts in middle to late Miocene sands in southwestern Montana (Fritz & Sears, 1993; Sears & Ryan, 2003) were sourced from central Idaho, suggesting northeastward drainage from central Idaho (Beranek et al., 2006). Beranek et al. (2006) show this capture occurring near the confluence between the Salmon and North Fork Salmon Rivers sometime between 4 and 2 Ma (Figures 9 and 10 in Beranek et al., 2006). Based on the sharp westward turn in the Salmon River near this confluence (NF Salmon in Figure 1a), Anderson (1947) similarly suggested that this sharp turn was caused by drainage capture "by headward erosion of a vigorous stream from the west." Although Anderson's hypothesis is qualitative, it is possible this western stream's vigor was caused by the rock-uplift variations proposed by Larimer et al. (2018). Much like the drainage capture scenarios we consider (Figure 12), drainage capture along the upper Salmon River would cause incision that decreases downstream. This capture event could be an additional signal in this landscape. If this drainage capture was precipitated only by the drainage of Lake Idaho, without any change in rock uplift, it cannot explain why high k_{sn} would be maintained along the lower reaches of the Salmon River and its tributaries.

While there are active Quaternary faults in the region (Figure 2; U.S. Geological Survey and Idaho Geological Survey, 2018), the locations and magnitudes of throw (Garwood et al., 2008) do not explain the incision patterns we observe here. An increase in rock uplift could be achieved through a range of alternative drivers, however. One possibility is that flexural isostasy is ongoing due to the region's suspected lithospheric loss (Camp & Hanan, 2008; Darold & Humphreys, 2013; Hales et al., 2005), as proposed by Larimer et al. (2018). These authors also modeled the flexure of an elastic plate subjected to a buoyant load to demonstrate that density changes extending 200 km north of the Snake River Plain could cause the proposed northward surface tilting. This hypothesis is also supported by tomography data showing (1) a high-velocity structure near the Yellowstone plume that may represent lithospheric downwelling (Yuan & Dueker, 2005) and (2) significantly slower mantle seismic velocities along the 44th parallel in central Idaho potentially indicative of the replacement of lithosphere by warmer mantle (Shen et al., 2013). Such interactions are already suspected in this region, as the Yellowstone plume may have aided in (1) the detachment of a dense plutonic root from the Wallowa Mountains in NE Oregon (Figure 1a; Hales et al., 2005) and/or (2) the delamination of remnant Farallon oceanic lithosphere from the base of NE Oregon (Darold & Humphreys, 2013). Indeed, Camp and Hanan (2008) argue that a plume-triggered delamination satisfies the geochemical characteristics of CRB flows over time. The Wallowa Mountains are situated far from much of our study area, however, and delamination would likely coincide with volcanism (Kay & Kay, 1993; Manley et al., 2000); besides the CRBs, no recent (<20 Ma) volcanism is documented in much of our study area. Regional uplift could also be provided through buoyant support from the Yellowstone plume (Pierce & Morgan, 1992; Vogl et al., 2014). Indeed, the trend we observe here of decreasing knickpoint elevations and incision depths toward the north, and away from the Yellowstone hotspot track, makes the involvement of the Yellowstone plume an interesting prospect. If the Yellowstone plume has contributed to increased rock-uplift rates, then the northern US Cordillera could be one of the best locations to examine the role of mantle dynamics in landscape evolution.

6. Conclusions

Bedrock river morphologies in central Idaho show that landscape transience in the region may be driven by spatially varying rock uplift, as proposed by Larimer et al. (2018). These findings are supported by the north to south increase in both knickpoint elevations (Figures 7–9) and transient incision depths (Figures 7, 8, and 10) across the Clearwater and Salmon watersheds. Knickpoint elevations range from about 800 to 2,200 m, while incision depths along main drainages range from about 300 to 1,200 m and increase by 3.93 m per km south ($R^2 = 0.7$). Enhanced rock-uplift rates may be higher and/or longer sustained to the south. We support these interpretations with an analytical model of transient bedrock river behavior and example numerical models demonstrating that (1) knickpoint elevations and incision depths have different relationships with drivers of landscape evolution and (2) these differences can be exploited in the interpretation of transient landscapes. By focusing on individual tributaries, we show that patterns of rock uplift can be recognized

even in lithologically diverse settings. Enhanced rock uplift in the northern US Cordillera could be influenced by the Yellowstone plume and its facilitation of lithospheric foundering and subsequent flexural isostasy.

Acknowledgments
This work was supported by (1) the Thornbury Fellowship at Indiana University's Department of Earth and Atmospheric Sciences and (2) a grant from the National Science Foundation (NSF EAR-1727139). This research was supported in part by Lilly Endowment, Inc., through its support for the Indiana University Pervasive Technology Institute. This study's data are available in the IUScholarWorks digital repository at Indiana University (https://hdl.handle.net/2022/22681).

References

Amerson, B. E., Montgomery, D. R., & Meyer, G. (2008). Relative size of fluvial and glaciated valleys in central Idaho. *Geomorphology*, *93*(3-4), 537–547. https://doi.org/10.1016/j.geomorph.2007.04.001

Anderson, A. L. (1947). Drainage diversion in the northern Rocky Mountains of east-central Idaho. *The Journal of Geology*, *55*(2), 61–75. https://doi.org/10.1086/625402

Barry, T. L., Kelley, S. P., Reidel, S. P., Camp, V. E., Self, S., Jarboe, N. A., & Renne, P. R. (2013). Eruption chronology of the Columbia River Basalt Group. In S. P. Reidel, V. E. Camp, M. E. Ross, J. A. Wolff, B. S. Martin, T. L. Tolan, & R. Wells (Eds.), *The Columbia River flood basalt province*, *Geological Society of America Special Papers* (Vol. 497, pp. 45–66). https://doi.org/10.1130/2013.2497(02)

Beranek, L. P., Link, P. K., & Fanning, C. M. (2006). Miocene to Holocene landscape evolution of the western Snake River Plain region, Idaho: Using the SHRIMP detrital zircon provenance record to track eastward migration of the Yellowstone hotspot. *Geological Society of America Bulletin*, *118*(9–10), 1027–1050.

Berlin, M. M., & Anderson, R. S. (2007). Modeling of knickpoint retreat on the Roan Plateau, western Colorado. *Journal of Geophysical Research*, *112*, F03SO6. https://doi.org/10.1029/2006JF000553

Bishop, P. (2007). Long-term landscape evolution: Linking tectonics and surface processes. *Earth Surface Processes and Landforms*, *32*(3), 329–365. https://doi.org/10.1002/esp.1493

Bishop, P., & Goldrick, G. (2010). Lithology and the evolution of bedrock rivers in post-orogenic settings: Constraints from the high-elevation passive continental margin of SE Australia. *Geological Society, London, Special Publications*, *346*(1), 267–287. https://doi.org/10.1144/SP346.14

Bishop, P., Hoey, T. B., Jansen, J. D., & Artza, I. L. (2005). Knickpoint recession rate and catchment area: The case of uplifted rivers in eastern Scotland. *Earth Surface Processes and Landforms*, *30*(6), 767–778. https://doi.org/10.1002/esp.1191

Braun, J. (2010). The many surface expressions of mantle dynamics. *Nature Geoscience*, *3*(12), 825–833. https://doi.org/10.1038/ngeo1020

Bursztyn, N., Pederson, J. L., Tressler, C., Mackley, R. D., & Mitchell, K. J. (2015). Rock strength along a fluvial transect of the Colorado Plateau—Quantifying a fundamental control on geomorphology. *Earth and Planetary Science Letters*, *429*, 90–100. https://doi.org/10.1016/j.epsl.2015.07.042

Camp, V. E., & Hooper, P. R. (1981). Geologic studies of the Columbia Plateau: Part I. Late Cenozoic evolution of the southeast part of the Columbia River Basalt Province. *GSA Bulletin*, *92*(9), 659–668. https://doi.org/10.1130/0016-7606(1981)92<659:GSOTCP>2.0.CO;2

Camp, V. E., Hooper, P. R., Swanson, D. A., & Wright, T. L. (1982). Columbia River basalt in Idaho: Physical and chemical characteristics, flow distribution, and tectonic implications. *Cenozoic Geology of Idaho: Idaho Bureau of Mines and Geology Bulletin*, *25*, 55–75.

Camp, V. E., & Hanan, B. B. (2008). A plume-triggered delamination origin for the Columbia River Basalt Group. *Geosphere*, *4*(3), 480–495. https://doi.org/10.1130/GES00175.1

Carretier, S., Nivière, B., Giamboni, M., & Winter, T. (2006). Do river profiles record along-stream variations of low uplift rate? *Journal of Geophysical Research*, *111*, F02024. https://doi.org/10.1029/2005JF000419

Coffin, M., & Eldholm, O. (1994). Large igneous provinces: Crustal structure, dimensions, and external consequences. *Reviews of Geophysics*, *32*(1), 1–36. https://doi.org/10.1029/93RG02508

Crosby, B. T., & Whipple, K. X. (2006). Knickpoint initiation and distribution within fluvial networks: 236 waterfalls in the Waipaoa River, North Island, New Zealand. *Geomorphology*, *82*(1–2), 16–38. https://doi.org/10.1016/j.geomorph.2005.08.023

Darold, A., & Humphreys, E. (2013). Upper mantle seismic structure beneath the Pacific Northwest: A plume-triggered delamination origin for the Columbia River flood basalt eruptions. *Earth and Planetary Science Letters*, *365*, 232–242. https://doi.org/10.1016/j.epsl.2013.01.024

DiBiase, R. A., & Whipple, K. X. (2011). The influence of erosion thresholds and runoff variability on the relationships among topography, climate, and erosion rate. *Journal of Geophysical Research*, *116*, F04036. https://doi.org/10.1029/2011JF002095

Dickinson, W. R. (2004). Evolution of the North American cordillera. *Annual Review of Earth and Planetary Sciences*, *32*(1), 13–45. https://doi.org/10.1146/annurev.earth.32.101802.120257

Duvall, A., Kirby, E., & Burbank, D. (2004). Tectonic and lithologic controls on bedrock channel profiles and processes in coastal California. *Journal of Geophysical Research*, *109*, F03002. https://doi.org/10.1029/2003JF000086

England, P., & Molnar, P. (1990). Surface uplift, uplift of rocks, and exhumation of rocks. *Geology*, *18*(12), 1173–1177. https://doi.org/10.1130/0091-7613(1990)018<1173:SUUORA>2.3.CO;2

Finnegan, N. J., Roe, G., Montgomery, D. R., & Hallet, B. (2005). Controls on the channel width of rivers: Implications for modeling fluvial incision of bedrock. *Geology*, *33*(3), 229–232. https://doi.org/10.1130/G21171.1

Flint, J. J. (1974). Stream gradient as a function of order, magnitude, and discharge. *Water Resources Research*, *10*(5), 969–973. https://doi.org/10.1029/WR010i005p00969

Forte, A. M., Yanites, B. J., & Whipple, K. X. (2016). Complexities of landscape evolution during incision through layered stratigraphy with contrasts in rock strength. *Earth Surface Processes and Landforms*, *41*(12), 1736–1757. https://doi.org/10.1002/esp.3947

Fritz, W. J., & Sears, J. W. (1993). Tectonics of the Yellowstone hotspot wake in, southwestern Montana. *Geology*, *21*(5), 427–430. https://doi.org/10.1130/0091-7613(1993)021<0427:TOTYHW>2.3.CO;2

Gallen, S. F. (2018). Lithologic controls on landscape dynamics and aquatic species evolution in post-orogenic mountains. *Earth and Planetary Science Letters*, *493*, 150–160. https://doi.org/10.1016/j.epsl.2018.04.029

Gallen, S. F., Wegmann, K. W., & Bohnenstieh, D. R. (2013). Miocene rejuvenation of topographic relief in the southern Appalachians. *GSA Today*, *23*(2), 4–10. https://doi.org/10.1130/GSATG163A.1

Garwood, D. L., Schmidt, K. L., Kauffman, J. D., Stewart, D. E., Lewis, R. S., Othberg, K. L., & Wampler, P. J. (2008). Geologic map of the White Bird Quadrangle, Idaho County, Idaho. Geologic Map, White Bird, Idaho: Idaho Geological Survey.

Gasparini, N. M., & Whipple, K. X. (2014). Diagnosing climatic and tectonic controls on topography: Eastern flank of the northern Bolivian Andes. *Lithosphere*, *6*(4), 230–250. https://doi.org/10.1130/L322.1

Goren, L. (2016). A theoretical model for fluvial channel response time during time-dependent climatic and tectonic forcing and its inverse applications. *Geophysical Research Letters*, *43*, 10,753–10,763. https://doi.org/10.1002/2016GL070451

Hack, J. T. (1957). Studies of longitudinal stream profiles in Virginia and Maryland. US Government Printing Office, 294.
Hack, J. T. (1973). Stream-profile analysis and stream-gradient index. *Journal Research of the US Geological Survey*, *1*(4), 421–429.
Hales, T. C., Abt, D. L., Humphreys, E. D., & Roering, J. J. (2005). A lithospheric instability origin for Columbia River flood basalts and Wallowa Mountains uplift in northeast Oregon. *Nature*, *438*(7069), 842–845. https://doi.org/10.1038/nature04313
Hamilton, W. B. (1963). *Metamorphism in the Riggins region, Western Idaho* (*USGS Numbered Series* Vol. 436). Washington, DC: U.S. Gov. Print. Off. Retrieved from http://pubs.er.usgs.gov/publication/pp436
Han, J., Gasparini, N. M., Johnson, J. P. L., & Murphy, B. P. (2014). Modeling the influence of rainfall gradients on discharge, bedrock erodibility, and river profile evolution, with application to the Big Island, Hawai'i. *Journal of Geophysical Research: Earth Surface*, *119*, 1418–1440. https://doi.org/10.1002/2013JF002961
Hancock, G. S., Anderson, R. S., & Whipple, K. X. (1998). Beyond power: Bedrock river incision process and form. In K. J. Tinkler, & E. E. Wohl (Eds.), *Rivers over rock: Fluvial processes in bedrock channels*, *Geophysical Monograph Series* (Vol. 107, pp. 35–60). Washington, DC: American Geophysical Union. https://doi.org/10.1029/GM107p0035
Harkins, N., Kirby, E., Heimsath, A., Robinson, R., & Reiser, U. (2007). Transient fluvial incision in the headwaters of the Yellow River, northeastern Tibet, China. *Journal of Geophysical Research*, *112*, F03S04. https://doi.org/10.1029/2006JF000570
Hergarten, S., Robl, J., & Stüwe, K. (2015). Tectonic geomorphology at small catchment sizes—Extensions of the stream-power approach and the χ method. *Earth Surface Dynamics Discussions*, *3*(3), 689–714. https://doi.org/10.5194/esurfd-3-689-2015
Hilley, G. E., & Arrowsmith, J. R. (2008). Geomorphic response to uplift along the Dragon's Back pressure ridge, Carrizo Plain, California. *Geology*, *36*(5), 367–370. https://doi.org/10.1130/G24517A.1
Howard, A. D. (1994). A detachment-limited model of drainage basin evolution. *Water Resources Research*, *30*(7), 2261–2285. https://doi.org/10.1029/94WR00757
Howard, A. D., & Kerby, G. (1983). Channel changes in badlands. *Geological Society of America Bulletin*, *94*(6), 739–752. https://doi.org/10.1130/0016-7606(1983)94<739:CCIB>2.0.CO;2
Janecke, S. U. (1992). Kinematics and timing of three superposed extensional systems, east central Idaho: Evidence for an Eocene tectonic transition. *Tectonics*, *11*(6), 1121–1138. https://doi.org/10.1029/92TC00334
Janecke, S. U., & Blankenau, J. J. (2003). Extensional folds associated with Paleogene detachment faults in SE part of the Salmon Basin. *Northeastern Geology*, *32*, 51–73.
Janecke, S. U., Geissman, J. W., & Bruhn, R. L. (1991). Localized rotation during Paleogene Extension in east central Idaho: Paleomagnetic and geologic evidence. *Tectonics*, *10*(2), 403–432. https://doi.org/10.1029/90TC02465
Kasbohm, J., & Schoene, B. (2018). Rapid eruption of the Columbia River flood basalt and correlation with the mid-Miocene climate optimum. *Science Advances*, *9*, eaat8223. https://doi.org/10.1126/sciadv.aat8223
Kay, R. W., & Kay, S. M. (1993). Delamination and delamination magmatism. *Tectonophysics*, *219*(1–3), 177–189. https://doi.org/10.1016/0040-1951(93)90295-U
Lague, D. (2014). The stream power river incision model: Evidence, theory and beyond. *Earth Surface Processes and Landforms*, *39*(1), 38–61. https://doi.org/10.1002/esp.3462
Larimer, J. E., Yanites, B. J., Phillips, W., & Mittelstaedt, E. (2018). Late Miocene rejuvenation of central Idaho landscape evolution: A case for surface processes driven by plume-lithosphere interaction. *Lithosphere*, *10*(6), 14. https://doi.org/10.1130/L746.1
Lewis, R. S., Link, P. K., Stanford, L. R., & Long, S. P. (2012). Geologic map of Idaho—Idaho Geological Survey. Retrieved from [https://www.idahogeology.org/product/m-9].
Link, P. K., Crosby, B. T., Lifton, Z. M., Eversole, E. A., & Rittenour, T. M. (2014). The late Pleistocene (17 ka) Soldier Bar landslide and Big Creek Lake, Frank Church—River of no return wilderness, Central Idaho, U.S.A. *Rocky Mountain Geology*, *49*(1), 17–31.
Lund, K., Snee, L. W., & Evans, K. V. (1986). Age and genesis of precious metals deposits, Buffalo Hump District, central Idaho; Implications for depth of emplacement of quartz veins. *Economic Geology*, *81*(4), 990–996. https://doi.org/10.2113/gsecongeo.81.4.990
Manley, C. R., Glazner, A. F., & Farmer, G. L. (2000). Timing of volcanism in the Sierra Nevada of California: Evidence for Pliocene delamination of the batholithic root?*Geology*, *28*, 811–814. https://doi.org/10.1130/0091-7613(2000)28<811:TOVITS>2.0.CO;2
Meyer, G. A., & Leidecker, M. E. (1999). Fluvial terraces along the Middle Fork Salmon River, Idaho, and their relation to glaciation, landslide dams, and incision rates: A preliminary analysis and river-mile guide. In S. S. Hughes, & G. D. Thackray (Eds.), *Guidebook to the geology of Eastern Idaho* (pp. 219–235). Pocatello, Idaho: Idaho Museum of Natural History.
Miller, S. R., Sak, P. B., Kirby, E., & Bierman, P. R. (2013). Neogene rejuvenation of central Appalachian topography: Evidence for differential rock uplift from stream profiles and erosion rates. *Earth and Planetary Science Letters*, *369–370*, 1–12. https://doi.org/10.1016/j.epsl.2013.04.007
Molnar, P., & England, P. (1990). Late Cenozoic uplift of mountain ranges and global climate change: Chicken or egg? *Nature*, *346*(6279), 29–34. https://doi.org/10.1038/346029a0
Montgomery, D., & Foufoula-Georgiou, E. (1993). Channel network source representation using digital elevation models—Montgomery—1993—Water Resources Research—Wiley Online Library. Retrieved from [https://agupubs-onlinelibrary-wiley-com.proxyiub.uits.iu.edu/doi/abs/10.1029/93WR02463]
Montgomery, D., & Gran, K. (2001). Downstream variations in the width of bedrock channels. *Water Resources Research*, *37*(6), 1841–1846. https://doi.org/10.1029/2000WR900393
Morriss, M. C., & Wegmann, K. W. (2017). Geomorphology of the Burnt River, eastern Oregon, USA: Topographic adjustments to tectonic and dynamic deformation. *Geomorphology*, *278*, 43–59. https://doi.org/10.1016/j.geomorph.2016.09.015
Mudd, S. M., Attal, M., Milodowski, D. T., Grieve, S. W. D., & Valters, D. A. (2014). A statistical framework to quantify spatial variation in channel gradients using the integral method of channel profile analysis. *Journal of Geophysical Research: Earth Surface*, *119*, 138–152. https://doi.org/10.1002/2013JF002981
Mudd, S. M., Clubb, F. J., Gailleton, B., & Hurst, M. D. (2018). How concave are river channels?*Earth Surface Dynamics*, *6*(2), 505–523. https://doi.org/10.5194/esurf-6-505-2018
Murphy, B. P., Johnson, J. P. L., Gasparini, N. M., & Sklar, L. S. (2016). Chemical weathering as a mechanism for the climatic control of bedrock river incision. *Nature*, *532*(7598), 223–227. https://doi.org/10.1038/nature17449
Niemann, J. D., Gasparini, N. M., Tucker, G. E., & Bras, R. L. (2001). A quantitative evaluation of Playfair's law and its use in testing long-term stream erosion models. *Earth Surface Processes and Landforms*, *26*(12), 1317–1332. https://doi.org/10.1002/esp.272
Olsen, P. E. (1997). Stratigraphic record of the Early Mesozoic breakup of Pangea in the Laurasia-Gondwana rift system. *Annual Review of Earth and Planetary Sciences*, *25*(1), 337–401. https://doi.org/10.1146/annurev.earth.25.1.337

Parker, C. (2016). Baseline erosion rates for the Fernan watershed inferred from cosmogenic ^{10}Be concentrations: Comparing erosion and sediment yields over different time-scales, (Masters of Science). Retrieved from [https://search-proquest-com.proxyiub.uits.iu.edu/docview/1850224892?pq-origsite=gscholar]. Moscow, ID: University of Idaho.

Perne, M., Covington, M. D., Thaler, E. A., & Myre, J. M. (2017). Steady state, erosional continuity, and the topography of landscapes developed in layered rocks. *Earth Surface Dynamics*, *5*(1), 85–100. https://doi.org/10.5194/esurf-5-85-2017

Perron, J. T., & Royden, L. (2013). An integral approach to bedrock river profile analysis. *Earth Surface Processes and Landforms*, *38*(6), 570–576. https://doi.org/10.1002/esp.3302

Pierce, K. L., & Morgan, L. A. (1992). The track of the Yellowstone hot spot: Volcanism, faulting, and uplift. *Regional Geology of Eastern Idaho and Western Wyoming: Geological Society of America Memoir*, *179*(322), 1–53. https://doi.org/10.1130/MEM179-p1

Royden, L., & Perron, T. (2013). Solutions of the stream power equation and application to the evolution of river longitudinal profiles. *Journal of Geophysical Research: Earth Surface*, *118*, 497–518. https://doi.org/10.1002/jgrf.20031

Saleeby, J. B. (1983). Accretionary tectonics of the north American cordillera. *Annual Review of Earth and Planetary Sciences*, *11*(1), 45–73. https://doi.org/10.1146/annurev.ea.11.050183.000401

Schoenbohm, L. M., Whipple, K. X., Burchfiel, B. C., & Chen, L. (2004). Geomorphic constraints on surface uplift, exhumation, and plateau growth in the Red River region, Yunnan Province, China. *Geological Society of America Bulletin*, *116*(7), 895–909. https://doi.org/10.1130/B25364.1

Schwanghart, W., & Scherler, D. (2014). Short communication: TopoToolbox 2—MATLAB-based software for topographic analysis and modeling in Earth surface sciences. *Earth Surface Dynamics*, *2*(1), 1–7. https://doi.org/10.5194/esurf-2-1-2014

Schwanghart, W., & Kuhn, N. J. (2010). TopoToolbox: A set of Matlab functions for topographic analysis. *Environmental Modelling & Software*, *25*(6), 770–781. https://doi.org/10.1016/j.envsoft.2009.12.002

Sears, J. W., & Ryan, P. C. (2003). Cenozoic evolution of the Montana Cordillera: Evidence from paleovalleys, (pp. 289–301). Retrieved from [http://archives.datapages.com.proxyiub.uits.iu.edu/data/rocky_sepm/data/036/036001/289_rocky_mount360289.htm]. Rocky Mountain Section (SEPM)

Shen, W., Ritzwoller, M. H., & Schulte-Pelkum, V. (2013). A 3-D model of the crust and uppermost mantle beneath the Central and Western US by joint inversion of receiver functions and surface wave dispersion. *Journal of Geophysical Research: Solid Earth*, *118*, 262–276. https://doi.org/10.1029/2012JB009602

Sklar, L. S., & Dietrich, W. E. (2001). Sediment and rock strength controls on river incision into bedrock. *Geology*, *29*(12), 1087–1090. https://doi.org/10.1130/0091-7613(2001)029<1087:SARSCO>2.0.CO;2

Snee, L. W., Lund, K., Sutter, J. F., Balcer, D. E., & Evans, K. V. (1984). The Salmon River Suture Zone, Western Idaho. US Geological Survey Professional Paper, 1438, 359–414.

Sonder, L. J., & Jones, C. H. (1999). Western United States extension: How the west was widened. *Annual Review of Earth and Planetary Sciences*, *27*(1), 417–462. https://doi.org/10.1146/annurev.earth.27.1.417

Sweetkind, D. S., & Blackwell, D. D. (1989). Fission-track evidence of the Cenozoic thermal history of the Idaho batholith. *Tectonophysics*, *157*(4), 241–250. https://doi.org/10.1016/0040-1951(89)90142-X

Tarboton, D. G., Bras, R. L., & Rodriguez-Iturbe, I. (1991). On the extraction of channel networks from digital elevation data. *Hydrological Processes*, *5*(1), 81–100. https://doi.org/10.1002/hyp.3360050107

Tikoff, B., Kelso, P., Manduca, C., Markley, M. J., & Gillaspy, J. (2001). Lithospheric and crustal reactivation of an ancient plate boundary: The assembly and disassembly of the Salmon River suture zone, Idaho, USA. *Geological Society, London, Special Publications*, *186*(1), 213–231. https://doi.org/10.1144/GSL.SP.2001.186.01.13

Tucker, G. E., & Whipple, K. X. (2002). Topographic outcomes predicted by stream erosion models: Sensitivity analysis and intermodel comparison. *Journal of Geophysical Research*, *107*(B9), 2179. https://doi.org/10.1029/2001JB000162

Turowski, J. M., Lague, D., & Hovius, N. (2009). Response of bedrock channel width to tectonic forcing: Insights from a numerical model, theoretical considerations, and comparison with field data. *Journal of Geophysical Research*, *114*, F03016. https://doi.org/10.1029/2008JF001133

U.S. Geological Survey and Idaho Geological Survey (2018). Quaternary fault and told database for the United States. Retrieved from [https://earthquake.usgs.gov/hazards/qfaults/]

Vogl, J. J., Min, K., Carmenate, A., Foster, D. A., & Marsellos, A. (2014). Miocene regional hotspot-related uplift, exhumation, and extension north of the Snake River Plain: Evidence from apatite (U-Th)/He thermochronology. *Lithosphere*, *6*(2), 108–123. https://doi.org/10.1130/L308.1

Wang, Y., Zhang, H., Zheng, D., Yu, J., Pang, J., & Ma, Y. (2017). Coupling slope-area analysis, integral approach and statistic tests to steady-state bedrock river profile analysis. *Earth Surface Dynamics*, *5*(1), 145–160. https://doi.org/10.5194/esurf-5-145-2017

Whipple, K. X. (2004). Bedrock rivers and the geomorphology of active Orogens. *Annual Review of Earth and Planetary Sciences*, *32*(1), 151–185. https://doi.org/10.1146/annurev.earth.32.101802.120356

Whipple, K. X., DiBiase, R. A., & Crosby, B. T. (2013). 9.28 Bedrock rivers. In J. F. Shroder (Ed.), *Treatise on geomorphology* (pp. 550–573). San Diego, CA: Academic Press. https://doi.org/10.1016/B978-0-12-374739-6.00254-2

Whipple, K. X., DiBiase, R. A., Ouimet, W. B., & Forte, A. M. (2017). Preservation or piracy: Diagnosing low-relief, high-elevation surface formation mechanisms. *Geology*, *45*(1), 91–94. https://doi.org/10.1130/G38490.1

Whipple, K. X., Forte, A. M., DiBiase, R. A., Gasparini, N. M., & Ouimet, W. B. (2017). Timescales of landscape response to divide migration and drainage capture: Implications for the role of divide mobility in landscape evolution. *Journal of Geophysical Research: Earth Surface*, *122*, 248–273. https://doi.org/10.1002/2016JF003973

Whipple, K. X., Hancock, G. S., & Anderson, R. S. (2000). River incision into bedrock: Mechanics and relative efficacy of plucking, abrasion, and cavitation. *GSA Bulletin*, *112*(3), 490–503. https://doi.org/10.1130/0016-7606(2000)112<490:RIIBMA>2.0.CO;2

Whipple, K. X., & Tucker, G. E. (1999). Dynamics of the stream-power river incision model: Implications for height limits of mountain ranges, landscape response timescales, and research needs. *Journal of Geophysical Research*, *104*(B8), 17,661–17,674. https://doi.org/10.1029/1999JB900120

Whittaker, A. C. (2012). How do landscapes record tectonics and climate? *Lithosphere*, *4*(2), 160–164. https://doi.org/10.1130/RF.L003.1

Whittaker, A. C., & Boulton, S. J. (2012). Tectonic and climatic controls on knickpoint retreat rates and landscape response times. *Journal of Geophysical Research*, *117*, F02024. https://doi.org/10.1029/2011JF002157

Whittaker, A. C., Cowie, P. A., Attal, M., Tucker, G. E., & Roberts, G. P. (2007). Contrasting transient and steady-state rivers crossing active normal faults: New field observations from the Central Apennines, Italy. *Basin Research*, *19*(4), 529–556. https://doi.org/10.1111/j.1365-2117.2007.00337.x

Willett, S. D. (1999). Orogeny and orography: The effect of erosion on the structure of mountain belts. *Journal of Geophysical Research*, *104*(B12), 28,957–28,981. https://doi.org/10.1029/1999JB900248

Wobus, C., Whipple, K. X., Kirby, E., Snyder, N., Johnson, J., Spyropolou, K., et al. (2006). Tectonics from topography: Procedures, promise, and pitfalls. In S. D. Willett, N. Hovius, M. T. Brandon, & D. M. Fisher (Eds.), *Tectonics, climate, and landscape evolution*, Special Paper (Vol. *398*, pp. 55–74). Boulder, CO: Geological Society of America, Inc. https://doi.org/10.1130/2006.2398(04)

Wohl, E., & David, G. C. L. (2008). Consistency of scaling relations among bedrock and alluvial channels. *Journal of Geophysical Research*, *113*, F04013. https://doi.org/10.1029/2008JF000989

Wood, S. H., & Clemens, D. M. (2002). Geologic and tectonic history of the western Snake River Plain, Idaho and Oregon. In B. Bonnichsen, C. M. White, & M. McCurry (Eds.), *Tectonic and magmatic evolution of the Snake River Plain volcanic province*, *Idaho Geological Survey Bulletin* (Vol. 30, pp. 69–103). Pocatello, ID: Idaho Academy of Science.

Wood, S. H. (1994). Seismic expression and geological significance of a lacustrine delta in Neogene deposits of the western Snake River plain, Idaho. *AAPG Bulletin*, *78*(1), 102–121.

Yanites, B. J. (2018). The dynamics of channel slope, width, and sediment in actively eroding bedrock river systems. *Journal of Geophysical Research: Earth Surface*, *123*, 1504–1527. https://doi.org/10.1029/2017JF004405

Yanites, B. J., Ehlers, T. A., Becker, J. K., Schnellmann, M., & Heuberger, S. (2013). High magnitude and rapid incision from river capture: Rhine River, Switzerland. *Journal of Geophysical Research: Earth Surface*, *118*, 1060–1084. https://doi.org/10.1002/jgrf.20056

Yanites, B. J., Tucker, G. E., Mueller, K. J., Chen, Y.-G., Wilcox, T., Huang, S.-Y., & Shi, K.-W. (2010). Incision and channel morphology across active structures along the Peikang River, central Taiwan: Implications for the importance of channel width. *GSA Bulletin*, *122*(7–8), 1192–1208. https://doi.org/10.1130/B30035.1

Yuan, H., & Dueker, K. (2005). Teleseismic *P*-wave tomogram of the Yellowstone plume. *Geophysical Research Letters*, *32*, L07304. https://doi.org/10.1029/2004GL022056

Zhou, Q., & Liu, L. (2019). Topographic evolution of the western United States since the early Miocene. *Earth and Planetary Science Letters*, *514*, 1–12. https://doi.org/10.1016/j.epsl.2019.02.029

Erratum

In the originally published version of this article, part of the line shown in Figure 6b was truncated due to a typesetting error. This has been corrected, and this may be considered the authoritative version of record.